Journal of Asian Earth Sciences xxx (2014) xxx–xxx

Contents lists available at ScienceDirect

Journal of Asian Earth Sciences

journal homepage: www.elsevier.com/locate/jseaes

Petrography and zircon U–Pb isotopic study of the Bayanwulashan Complex: Constrains on the Paleoproterozoic evolution of the Alxa Block, westernmost North China Craton

Sujuan Wu [a,b], Jianmin Hu [a,b,*], Minghua Ren [c], Wangbin Gong [a,b], Yang Liu [d], Jiyuan Yan [e]

[a] Institute of Geomechanics, Chinese Academy of Geological Sciences, Beijing 100081, China
[b] Key Laboratory of Paleomagnetism and Tectonic Reconstruction of Ministry of Land and Resources, Beijing 100081, China
[c] Department of Geoscience, University of Nevada, Las Vegas, Nevada 89154-4010, USA
[d] Kunming University of Science and Technology, Kunming 650093, China
[e] Shandong University of Science and Technology, Qingdao 266510, China

ARTICLE INFO

Article history:
Received 19 December 2013
Received in revised form 2 May 2014
Accepted 15 May 2014
Available online xxxx

Keywords:
Alxa Block
North China Craton
U–Pb zircon age
Paleoproterozoic
Petrography

ABSTRACT

The Bayanwulashan Metamorphic Complex (BMC) exposes along the eastern margin of the Alxa Block, the westernmost part of the North China Craton (NCC). BMC is principally composed of metamorphic rocks with amphibole plagiogneiss, biotite plagioclase gneiss and granitic gneiss. Our research has been focused on the petrography and zircon U–Pb geochronology of the BMC to better understand the evolution of the Alxa Block and its relationship with the NCC. Evidences from field geology, petrography, and mineral chemistry indicate that two distinct metamorphic assemblages, the amphibolite and greenschist facies, had overprinted the preexisting granitic gneiss and suggest that the BMC experienced retrograde metamorphic episodes. The LA-ICP-MS zircon U–Pb ages reveal that the primary magmatic activities of BMC were at ca. 2.30–2.24 Ga and the two metamorphic events were at ca. 1.95–1.91 Ga and ca. 1.88–1.85 Ga respectively. These ages indicate that BMC initially intruded during Paleoproterozoic, not as previously suggested at Archean period. The Early Paleoproterozoic metamorphic records and the magmatic thermochronological data in BMC exhibit different evolution paths between the Alxa Block and the NCC. The Alxa Block was most likely an independent Early Paleoproterozoic terrain. Following different amalgamation processes, The Alxa Block combined with Western Block at ca. 1.95 Ga and then united with NCC at ca. 1.85 Ga.

1. Introduction

The NCC is the largest and oldest Precambrian Craton in China. It has been divided into the Eastern and Western blocks (Zhao et al., 2005; Zhao, 2009; Zhao and Cawood, 2012). The Western Block includes subblocks of the Yinshan and Ordos, and the Eastern Block includes subblocks of the Longgang and Liaonan-Rangrim (Fig. 1). The Longgang and Liaonan-Rangrim blocks collided along the paleoproterozoic Jiao–Liao–Ji orogenic belts (Li et al., 2005, 2006, 2010, 2011, 2012a, 2012b; Li and Zhao, 2007). The Yinshan and the Ordos collided at 1.95–1.92 Ga and amalgamated into the Western Block along the Khondalite Belt (Zhao et al., 2005; Santosh et al., 2006, 2007a, 2007b, 2008; Wan et al., 2006; Xia et al., 2006a, 2006b; Wu et al., 2012, 2013). The Eastern and Western blocks collided along the Trans-North China Orogen (TNCO) at ~1.85 Ga and formed the basement of the NCC (Wilde et al., 2002; Zhao et al., 2004; Kröner et al., 2005; Santosh et al., 2010).

The Alxa block is located at the westernmost NCC and connects the Tarim Block to the west. It is largely covered by Cenozoic sedimentary deposits with Precambrian basement rocks being sporadically exposed in its eastern and southern parts. Compared with the other units of NCC, the Alxa Block has been poorly studied because of the sparse exposures and their unattainable locations. The lack of available information limits a broader understanding of the interdependence between the NCC and Alxa Block. The Alxa Block has generally been considered to collide with the NCC during the Proterozoic and constitute the western extension of the Yinshan Block (Ren et al., 1987; Wu et al., 1998; Geng et al., 2002; Zhao, 2009). Another hypothesis is that Alxa Block is part of the Khondalite Belt (Geng et al., 2007, 2010; Gong et al., 2012; Zhang et al., 2013). However, the recent zircon geochronology studies

* Corresponding author at: Institute of Geomechanics, Chinese Academy of Geological Sciences, Beijing 100081, China. Tel.: +86 (0)10 88815003; fax: 86 10 68422326.
E-mail address: jianminhu@vip.sina.com (J. Hu).

http://dx.doi.org/10.1016/j.jseaes.2014.05.011
1367-9120/

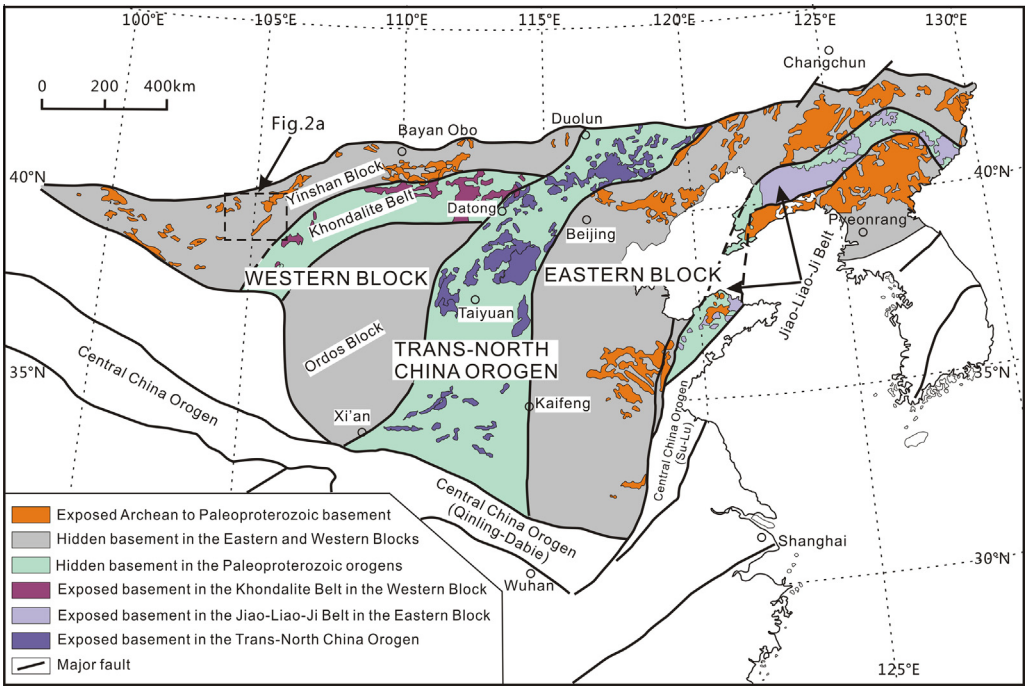

Fig. 1. Tectonic subdivision of the North China Craton (after Zhao et al., 2005) showing the distribution of the three continental blocks and two Paleoproterozoic orogenic belts in the NCC and the location of Alxa Block discussed in this paper.

for the basement and Paleozoic sediment of the Alxa Block (Li et al., 2012; Zhang et al., 2012; Dan et al.; 2012a; Yuan and Yang, 2013), the kinematics research (Zhang et al., 2013a, 2013b) and the paleomagnetic studies (Huang et al., 1999, 2000, 2001; Meng et al., 1990; Wu et al., 1993., Liu et al., 2010a, 2010b; Yuan and Yang, 2014) have all suggested that the Alxa Block and the NCC were the independent blocks prior to the Early–Middle Paleozoic.

No matter which model is correct, the petrography feature, the protolith age and metamorphism of the basement rocks can provide extremely important information for recognizing the evolutionary of the Alxa Block and the correlation between Alxa Block and NCC. Combined with previous data, the results of this study have provided important insights into the current understanding for the evolution of the Alxa Block.

2. Geological background

The Alxa Block is largely covered by Cenozoic sediments and the outcrops of Precambrian metamorphic basement rocks are only exposed in the southwestern and eastern parts of the block (Fig. 2a). The southwestern basement rocks, Longshoushan Complex, and the eastern basement rocks, Alashan Group, have been mapped as the Archean basement (NMBGMR, 1991). The Longshoushan Complex composes ca. 2.1–1.9 Ga amphibolite-facies metamorphosed igneous rocks and <1.72 Ga greenschist-facies meta-sedimentary rocks (Tung et al., 2007; Gong et al., 2011). In recent years, some authors have subdivided the traditional Alashan Group into three metamorphic and two deformed orthogenesis complexes: the Archean Diebusige Complex, the Paleoproterozoic Bayanwulashan Complex, the Paleo-Middle Proterozoic Alxa Complex, the Boluosutanmiao orthogneiss and the Bijiegetai orthogneiss (Geng et al., 2006a, 2007, 2010; Geng and Zhou, 2010) (Fig. 2a).

The NE-striking Bayanwula Mountain is situated along the eastern boundary of the Alxa Block (Fig. 2b). The Bayanwulashan Metamorphic Complex (BMC) is only exposed in the Bayanwula Mountain and is isolated from other Precambrian rocks. The BMC is a part of the Precambrian metamorphic Alxa Block and is principally composed of mafic and quartzo-feldspathic gneisses, intercalated with a few layered amphibolites and minor marbles (Geng et al., 2006a). In the central-southern part of the Bayanwula Mountain, the amphibolite has experienced retrogressed change and altered into sericite-chlorite-hornblende schists and albite-chlorite schists due to strong deformation (Geng et al., 2006a, 2007). The Paleoproterozoic period is important for the evolution of the Alxa Block and the NCC, but the detailed metamorphic history of the Alxa Block is still unclear because of the lack of reliable data. In the past decade, the isotopic geochronology data indicate that BMC was formed during the Archean to Early Paleoproterozoic (mostly at ca. 2.34–2.08 Ga) (Dan et al., 2012a; Dong et al., 2007; Geng et al., 2006a, 2007). The BMC underwent two metamorphic events in the Paleoproterozoic, but several authors have given different metamorphic ages at either ca. 1.89 Ga and 1.79 Ga, or ca. 1.92 Ga and ca. 1.86 Ga (Dan et al., 2012a; Dong et al., 2007). To clarify the geological history for this area, geochronological and geochemical analyses were conducted on the BMC in this study.

3. Sampling and Petrographical characteristics

Seven samples were collected from the BMC for this study and their locations are labeled in Fig. 2b. All the exposed rocks show high-grade metamorphism and intense polyphase deformation, some of them are mylonitized. The gneissic foliations are the main characteristics of those rocks. The foliation is defined by flattened and oriented quartzes, biotites and feldspar aggregates (Fig. 3).

- *Amphibole plagiogneiss (HT50-3, N39°40′57.2″, E105°15′13″; HT52-2, N39°36′47.1″, E105°08′35.5″)*

The amphibole plagiogneiss samples are composed of quartz (25–35%), plagioclase (35–40%), amphibole (10–25%), with minor K-feldspar, epidote, apatite, biotite and opaque minerals. Some amphiboles have been replaced by chlorite. These rocks show a mylonitic texture and gneissic structure. The mineral assemblage

Please cite this article in press as: Wu, S., et al. Petrography and zircon U–Pb isotopic study of the Bayanwulashan Complex: Constrains on the Paleoproterozoic evolution of the Alxa Block, westernmost North China Craton. Journal of Asian Earth Sciences (2014), http://dx.doi.org/10.1016/j.jseaes.2014.05.011

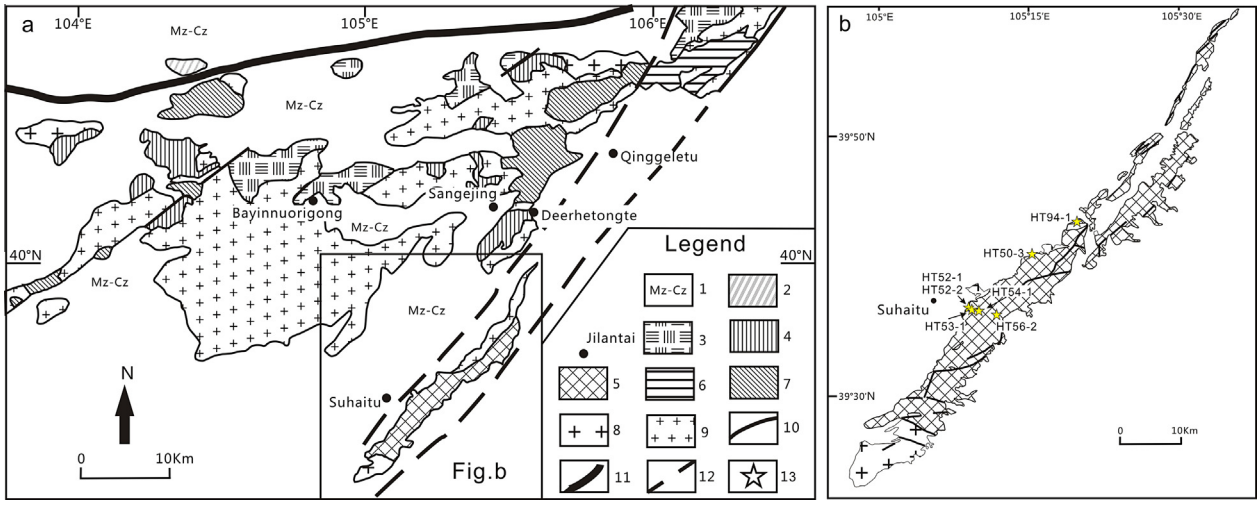

Fig. 2. Geological sketch map of the Alxa Block (after Geng et al., 2010) and Bayanwulashan Complex (modified after NMBGMR, 1991). (a) Shows the distributions of Precambrian basement rocks in the Alxa Block and adjacent areas; (b) showing the sample locations. 1. Meso-Cenozoic; 2. Paleozoic; 3. Mesoprotorozoic Bayinxibie Formation; 4. Paleo-and Mesoproterozoic Alxa Group;5. Paleoproterozoic Bayanwulashan Copmlex; 6. Neoarchean Diebusige Complex; 7. Plutonic metamorphic complex; 8. Boluosutanmiao tonalitic-granitic gneissic complex; 9. Hercynian-Indosinian granite;10. Fault; 11. Boundary fault; 12. 1nferred fault; 13. sample locations.

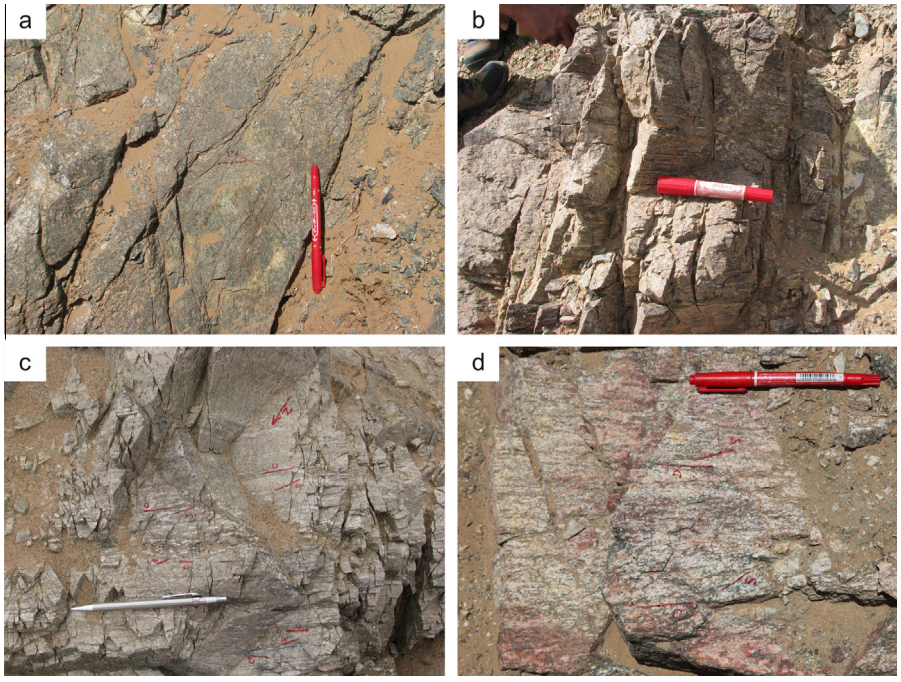

Fig. 3. Field photographs showing the major rocks from the Bayanwulashan. (a) Amphibole paagiogneiss; (b–c) granitic gneiss; and (d) biotite plagioclase gneiss.

of plagioclase + amphibole and the replacement of amphibole by chlorite + epidote indicate that these rocks underwent amphibolite facies metamorphism with subsequent overprinting of greenschist-facies metamorphism (Fig. 4a). The most significant feature of the rock is that the amphiboles have different chemistry, different shape, and orientated in different direction. Based on amphibole chemistry, they can be classified as tschermakite, actinolite and pargasite (Table 1, Fig. 4b) according to Leake (Leake et al., 1997, 2004) criteria. The pargasite are in blade shape with smaller grain size, and oriented nearly perpendicular to the foliation bends. The amphibole plagiogneiss should have experienced polyphase retrograde metamorphism (Fig. 4b).

- *Biotite plagioclase gneiss (HT53-1, N105°09′6.7″, E39°36′39.6″; HT54-1, N105°09′51.3″, E39°36′38.2″)*

The biotite plagioclase gneiss samples, HT53-1 and HT54-1, are composed of quartz (25–30%), plagioclase (35–40%), biotite (25–30%), epidote (3–5%) and sericite (<1%), with accessory minerals of apatite, magnetite and zircon. These rocks show evidence of strong deformation with elongated and oriented biotite, and undulatory extinction of quartzes (Fig. 4c and d).

- *Granitic gneiss (HT52-1, N39°36′47.1″, E105°08′35.5″)*

The granitic gneiss sample HT52-1 is composed of quartz (40%), plagioclase (40%), K-feldspar (5%), garnet (3%), chlorite (5%), titanite (1%) and calcite (<1%). All mineral are oriented parallel to the foliation. Quartz occurs in two forms: recrystallized quartz ribbon (Fig. 4e) and quartz associated with plagioclase. Quartz ribbons are the typical plastic deformation micro-fabrics in metamorphic rock,

Please cite this article in press as: Wu, S., et al. Petrography and zircon U–Pb isotopic study of the Bayanwulashan Complex: Constrains on the Paleoproterozoic evolution of the Alxa Block, westernmost North China Craton. Journal of Asian Earth Sciences (2014), http://dx.doi.org/10.1016/j.jseaes.2014.05.011

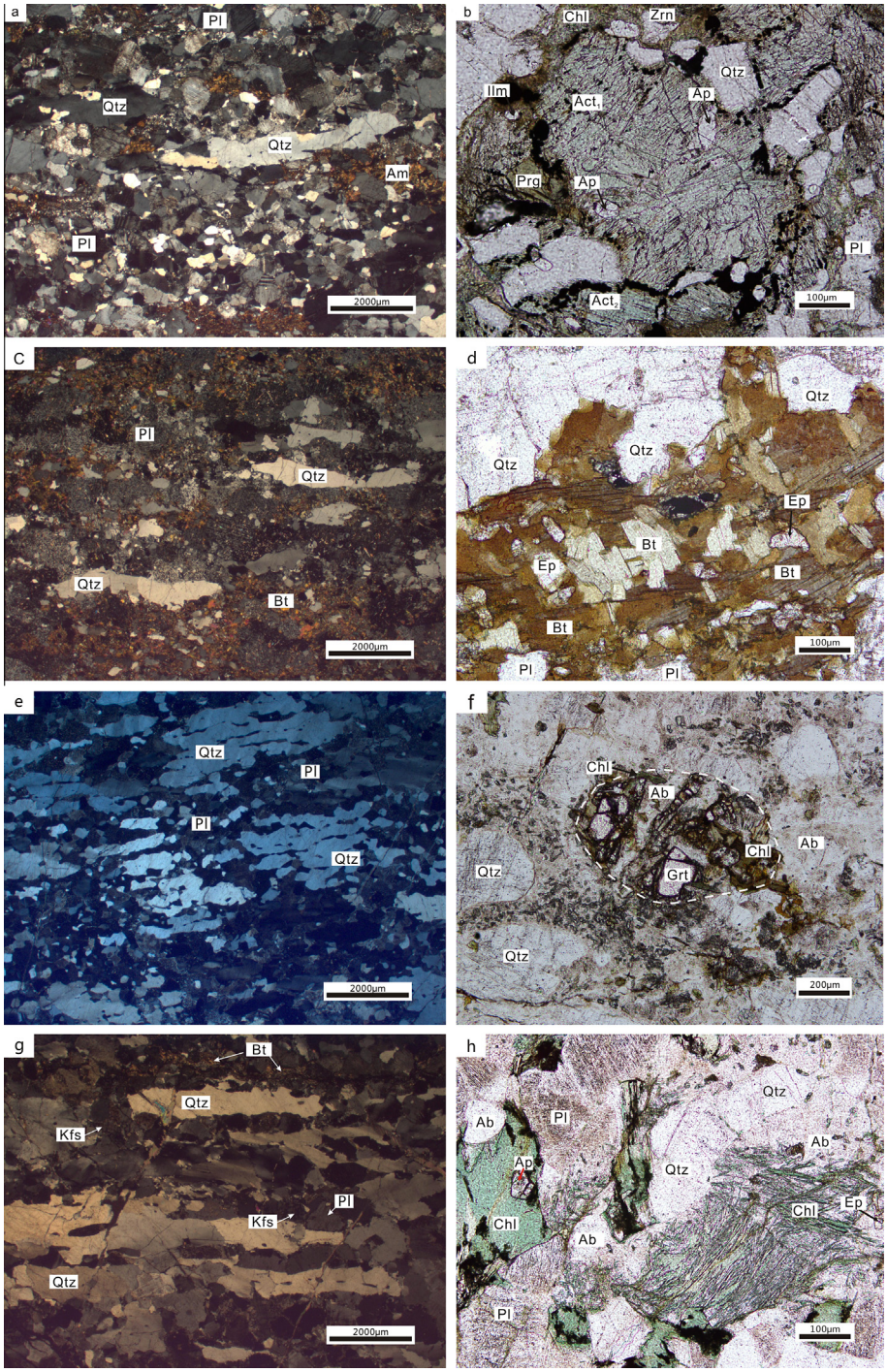

Fig. 4. Photomicrographs showing texture and mineral assemblages of rocks from the Bayanwulashan Complex. (a) Elongated coarse-grained recrystallized quartz bands are oriented to the foliation in amphibole plagioclase gneiss sample HT50-3; (b) minral assemblage of plagioclase and amphibole and the replacement of amphibole by chlorite and epidote in amphibole plagioclase gneiss HT52-2; (c–d) elongated and oriented biotite, and undulatory extinction of quartzes in biotite plagiogneiss sample HT53-1and HT54-1; (e) showing the two forms of quarta: recrystallized quartz ribbon and quartz associated with plagioclase in granitic gneiss sample HT52-1; (f) garnet grains were broken and only have a residue form in granitic gneiss sample HT52-1; (g) elongated coarse-grained rectystallized quartz bands oriented parallel to the foliation as defined by the orientation of biotite flakes, monzonite gneiss sample HT56-2; and (h) showing the mineral assemblage of albite + chlorite + epidote indicate that greeschist-facies metamorphism has been occurred in albite-chlorite schistsampel HT94-1. Mineral abbreviations: Pl-plagioclase; Qtz-quartz; Ap-apatite; Ep-epidote; Ilm-ilmenite; Mag-magnetite; Zrn-zircon; Chl-chlorite; Ttn-titanite; Bt-biotite; Prg- pargasite; Act- actinolite; Ts-tschermakite; Ab-albite; Grt-garnet (mineral abbreviation after Shen, 2009).

which are correlated to high temperature mylonite (Hippertt et al., 2001; Bochez, 1977). Because the rocks have undergone high-grade metamorphism and intense polyphase deformation, garnet grains were broken and only have a residue form (grain size varying from 0.5 to 1.5 mm) (Fig. 4f). The plagioclase and garnet underwent sericite and chlorite alteration, respectively.

- *Monzonite gneiss (HT56-2, N105°12′08.5″, E39°36′19.3″)*

The monzonite gneiss sample HT56-2 is composed of quartz (30%), plagioclase (35%), K-feldspar (25%), biotite (5%), chlorite (3%), epidote (<1%) and titanite (<1%), with accessory minerals of ilmenite, magnetite and zircon. This rock has similar mineral

Please cite this article in press as: Wu, S., et al. Petrography and zircon U–Pb isotopic study of the Bayanwulashan Complex: Constrains on the Paleoproterozoic evolution of the Alxa Block, westernmost North China Craton. Journal of Asian Earth Sciences (2014), http://dx.doi.org/10.1016/j.jseaes.2014.05.011

Table 1
Representative microprobe analyses of minerals from Bayanwulashan Complex (wt%).

Sample	Amphibole						Garnet					Biotite	
Mineral texture	HT50-3	HT50-3	HT50-3	HT50-3	HT52-2	HT52-2	HT52-1 Rim	HT52-1 Mantle	HT52-1 Mantle	HT52-1 Mantle	HT52-1 Rim	HT53-1	HT54-1
SiO_2	38.83	54.57	54.55	42.83	43.74	42.18	37.85	38.05	37.58	34.62	37.85	36.23	36.23
TiO_2	1.09	0.04	0.02	1.81	1.91	2.07	0.03	0.02	0.01	0	0.03	2.05	1.66
Al_2O_3	12.51	1.23	1.64	12.04	11.04	11	22.08	21.46	21.98	23.14	22.08	16.52	17.27
Cr_2O_3	0.08	0.03	0.03	0.09	0.04	0.01	0.04	0	0	0.01	0.04	0.05	0
FeO	3.59	9.43	9.55	14.23	16.61	17.62	29.79	29.51	30.2	26.87	29.79	19.86	21.91
MnO	0.13	0.41	0.41	0.12	0.32	0.35	3.14	3	3.08	11.07	3.14	0.28	0.26
MgO	11.19	16.07	15.83	11.14	9.79	8.54	4.67	4.97	4.54	1.27	4.67	9.86	8.88
CaO	9.62	12.09	11.94	11.8	11.94	11.57	3.9	3.95	3.94	3.85	3.9	0.15	0.01
Na_2O	1	0.17	0.22	1.57	1.42	1.4	0	0	0.03	0	0	0.08	0.06
K_2O	1.46	0.02	0.02	1.48	1.71	1.76	0.02	0	0	0.01	0.02	8.61	9.84
Total	93.82	96.94	97.65	98.33	100.18	98.6	101.6	101.04	101.45	101.03	101.6	93.7	96.13
O	23	23	23	23	23	23	12	12	12	12	12	11	11
Si	5.97	7.85	7.8	6.36	6.45	6.38	5.957	5.916	5.971	5.899	5.613	2.805	2.775
Ti	0.13	0	0	0.2	0.21	0.24	0.002	0.004	0.002	0.002	0	0.119	0.096
Al	2.26	0.21	0.28	2.11	1.92	1.96	4.029	4.068	3.969	4.066	4.422	1.508	1.559
Fe	2.05	1.44	1.5	1.84	2.21	2.45	3.93	3.893	3.872	3.965	3.643	1.286	1.404
Mg	2.56	3.45	3.37	2.46	2.15	1.93	1.062	1.089	1.163	1.062	0.308	1.138	1.013
Mn	0.02	0.05	0.05	0.02	0.04	0.05	0.406	0.415	0.399	0.409	1.52	0.018	0.017
Ca	1.58	1.86	1.83	1.88	1.89	1.88	0.641	0.653	0.665	0.663	0.668	0.012	0.001
Na	0.3	0.05	0.06	0.45	0.41	0.41	0.003	0	0.001	0.008	0.001	0.012	0.009
K	0.29	0	0	0.28	0.32	0.34	0.001	0.003	0	0	0.001	0.85	0.961
X_{Mg}	0.56	0.7	0.69	0.57	0.49	0.44	0.213	0.219	0.231	0.211	0.078	0.469	0.419
Pyr							17.588	18.001	19.066	17.415	5.014	–	–
Alm	–	–	–	–	–	–	65.072	64.338	63.488	65.004	59.347	–	–
Grs	–	–	–	–	–	–	10.613	10.796	10.901	10.877	10.881	–	–
Sps	–	–	–	–	–	–	6.727	6.865	6.545	6.704	24.759	–	–
Name	Ts	Act	Act	Prg	Prg	Fe-Prg	–	–	–	–	–	–	–

	Plagioclase												
	HT50-3	HT50-3	HT50-3	HT50-3	HT50-3	HT50-3	HT52-2	HT52-2	HT53-1	HT53-1	HT53-1	HT54-1	HT54-1
SiO_2	57.49	57.17	56.76	56.06	56.93	56.72	59.1	58.32	60.51	65.15	60.44	64.33	62.21
TiO_2	0	0	0	0	0.01	0	0.03	0.06	0.02	0	0	0	0
Al_2O_3	27.4	26.49	27.34	26.91	26.37	26.99	25.69	26.32	25.05	21.82	24.61	21.76	22.68
Cr_2O_3	0.01	0	0	0	0	0.01	0.02	0	0.01	0	0	0.01	0
FeO	0.25	0.13	0.14	0.18	0.19	0.14	0.19	0.18	0.23	0.08	0.13	0.02	0.15
MnO	0	0	0	0.02	0.02	0	0	0	0	0	0	0	0.01
MgO	0.01	0	0.01	0	0.03	0.01	0	0	0.01	0.01	0.01	0.01	0.02
CaO	9.31	8.53	9.15	9.09	7.73	8.71	7.53	7.81	6.07	2.48	5.99	2.75	4.04
Na_2O	6.12	6.21	6.11	6.19	5.44	6.29	7.08	6.8	7.86	9.55	7.77	9.46	8.35
K_2O	0.3	0.61	0.05	0.1	1.63	0.08	0.09	0.15	0.15	0.07	0.15	0.06	0.08
Total	100.95	99.24	99.69	98.66	98.39	98.96	99.73	99.69	99.91	99.3	99.13	98.43	97.62
O	8	8	8	8	8	8	8	8	8	8	8	8	8
Si	2.56	2.59	2.55	2.55	2.6	2.57	2.64	2.61	2.69	2.88	2.71	2.87	2.81
Ti	0	0	0	0	0	0	0	0	0	0	0	0	0
Al	1.44	1.41	1.45	1.44	1.42	1.44	1.35	1.39	1.31	1.14	1.3	1.14	1.21
Fe	0.01	0	0	0.01	0.01	0	0.01	0.01	0.01	0	0	0	0.01
Mg	0	0	0	0	0	0	0	0	0	0	0	0	0
Mn	0	0	0	0	0	0	0	0	0	0	0	0	0
Ca	0.44	0.41	0.44	0.44	0.38	0.42	0.36	0.38	0.29	0.12	0.29	0.13	0.2
Na	0.53	0.54	0.53	0.55	0.48	0.55	0.61	0.59	0.68	0.82	0.67	0.82	0.73
K	0.02	0.04	0	0.01	0.09	0	0	0.01	0.01	0	0.01	0	0
An mol%	44.87	41.63	45.14	44.56	39.6	43.14	36.85	38.48	29.66	12.49	29.62	13.76	21
Ab mol%	53.4	54.85	54.58	54.86	50.48	56.39	62.64	60.66	69.49	87.09	69.52	85.85	78.49
Or mol%	1.73	3.52	0.28	0.58	9.92	0.47	0.51	0.86	0.86	0.42	0.86	0.38	0.51

Abbreviations in this table: Prg-pargasite; Act-actinolite; Ts-tschermakite (mineral abbreviation after Shen, 2009).

assemblage to the sample HT52-1, but with larger minerals size and more K-feldspar and biotite. Biotite flakes are in contact with quartz and plagioclase. There are some elongated coarse-grain recrystallized quartz bands parallel to the foliation defined by the oriented biotite (Fig. 4g).

- *Albite -chlorite schist (HT94-1, N105°19′48.7″, E39°43′18.7″)*

The albite-chlorite schist sample HT94–1 consists of quartz (20%), plagioclase (50%), K-feldspar (5%), chlorite (15%), with minor epidote, titanite, apatite, and muscovite (Fig. 4h). Most plagioclase in this rock is albite (Table 1, see discussion in Section 5). The mineral assemblage of albite + chlorite + epidote indicates that this rock experienced greenschist-facies metamorphism.

4. Analytical procedures

4.1. Mineral chemistry

Detailed mineral chemistry studies were carried out on the electron microprobe analyses using the JEOL JAX8900 microprobe

Please cite this article in press as: Wu, S., et al. Petrography and zircon U–Pb isotopic study of the Bayanwulashan Complex: Constrains on the Paleoproterozoic evolution of the Alxa Block, westernmost North China Craton. Journal of Asian Earth Sciences (2014), http://dx.doi.org/10.1016/j.jseaes.2014.05.011

housed at the University of Nevada, Las Vegas. Electron beam conditions were 20 keV and 10 nA. Natural and synthetic silicates and oxides were used for calibration. Major cations were analyzed for all minerals. Matrix corrections used a ZAF correction program package on the JEOL 8900. Analytical precision based on replicate analyses of standards has standard deviation less than 0.5 for major and less than 0.1 for minor elements. Fe^{3+} was calculated by normalizing analyses to the respective cation total through charge balance considerations (Droop, 1987). Representative analytical data are presented in Table 1.

4.2. Zircon U–Pb dating

Zircons separated from six samples (HT50-3, HT52-1, HT52-2, HT53-1, HT54-1 and HT56-2) were dated using the laser ablation inductively coupled plasma mass spectrometry (LA-ICP-MS) U–Th–Pb isotopic method. Zircons were separated from approximate 2-kg rock samples by conventional magnetic and density techniques and then concentrated in heavy liquid fractions. Zircon grains were selected and processed by handpick separation procedure and were mounted in epoxy, which were then polished to expose the center of the crystals for analysis. All zircons were documented with transmitted and reflected light micrographs as well as cathodeluminescence (CL) images to reveal their internal structures.

The zircon U–Pb isotopes were analyzed using MC-ICPMS with a (ESI) UP193-FX ArF Excimer 193 nm wavelength laser ablation system at Tianjin Institute of Geology and Mineral Resources. The Neptune, Thermofisher Scientific, MC-ICP-MS instrument is equipped with nine Faraday cups, including an axial Faraday cup and eight off-axis Faraday cups, and four ion counters. Ablation was performed in a custom-designed chamber filled with Helium. The laser pulse rates are 8–10 Hz with a 35 μm beam size and the delivering energy is approximately 13–14 J/cm^{-2}. Mass bias, down hole fractionation, and instrumental drift were corrected by analyzing the Temora and GJ-1 international zircon standard (Black et al., 2003; Jackson et al., 2004) for every eight unknown zircon analyses. The NIST612 standard glass sample was used to calculate the Pb, U and Th contents. Data reductions were performed using the methods outlined by weighted averages. Concordia plots were calculated using the isoplot software of ICPMS DataCal by Liu et al. (2010a, 2010b) and Isoplot by Ludwig (2003). ^{208}Pb was applied for the common lead correction (Andersen, 2002). Individual analyses are presented with a 1σ error in data tables and in Concordia diagrams.

5. Mineral chemistry characteristics

Amphiboles have different types: tschermakite, actinolite, pargasite and Ferro-pargasite, according to Leake (Leake et al., 1997, 2004) classification criteria. The amphibole composition is very different in different textural settings. Tschermakite has oxide total of approx. 92.3%, and the oxide totals for other types of amphiboles are higher (95.32–99.97 wt.%). Tschermakite has the lowest SiO_2 content (38.8%), the highest Al_2O_3 content (12.5%), and the highest X_{Mg} (=0.85), the low total representing the presence of volatiles. Actinolite has the highest SiO_2 content, ranging from 44 to 56 wt.%, and the lowest TiO_2 and Al_2O_3 contents, ranging from 0.02 to 0.27 and 1.0 to 3.16, respectively. The actinolite X_{Mg} value ranges from 0.65 to 0.82. Ferro-pargasite has the highest FeO content, from 17.9 wt.% to 19.4 wt.%, and the lowest X_{Mg} value, ranging from 0.46 to 0.50. The pargasite X_{Mg} content ranges from 0.5 to 0.62. These compositional variations are comparable to previously reported ranges for amphibole compositions from amphiboles elsewhere on Alxa Block (Shen et al., 2004).

The feldspars found in these samples include plagioclase and albite, with minor k-feldspar in the felsic-rich leucosome domains. Plagioclase has the peak composition of $An_{36–46.6}$, $Ab_{50–55}$, $OR_{0.5–10}$ in amphibole plagiogneisses and the composition of $An_{12.5–30}$, $Ab_{69–87}$, $OR_{<1}$ in the biotite plagioclase gneisses. Albites are rare and are only found in samples HT52-1 and HT94-1. They typically occur in retrograde metamorphism and have high Ab values (95–99.3). K-feldspars found in the samples are fine-grained and show a composition of $Or_{92.5–99}$.

The garnets (grain size varying from 0.5 to 1.5 mm) are almandine-rich with $Alm_{51.1–69.7}$, $Prp_{2.3–19.4}$, $Sps_{6.2–37.6}$ and $Grs_{8.4–19.1}$. All analyzed garnet grains show nearly homogenous composition, although, in general, the rim portions are slightly enriched in X_{mn}. Because the rocks have undergone high-grade metamorphism and intense polyphase deformation, garnet grains were broken and only have a residue form (grain size varying from 0.5 to 1.5 mm). This study mainly collected the data in the narrow rim and the core. The garnets are almandine-rich (51.1–69.7 mol%) with minor pyrope (2.3–19.4 mol%), spessartine (3.2–37.6 mol%) and grossular (8.44–19.1 mol%). The garnet mantle is almandine-rich and has the highest Fe content ($Alm_{63.5–69.7}$, $Prp_{9.5–19.4}$, $Sps_{6.2–16}$, $Grs_{8.4–10.9}$ in mol%). The garnet rim is spessartine-rich and has the highest Mn content ($Alm_{51.1–60.8}$, $Prp_{2.3–5}$, $Sps_{24.5–37.6}$, $Grs_{8.8–19.1}$ in mol%). The weak compositional zoning and Mn enriched rim suggest that a diffusion reaction happened during the retrograde metamorphism (Kohn and Spear, 2000).

The composition of biotite in the samples is very similar in all textural settings. All the analyzed biotites have a slightly high-TiO_2 content ranging from 1.55 to 5.36 wt.%. The biotite X_{Mg} ranges from 0.42 to 0.57.

6. Zircon U–Pb dating results

6.1. Amphibole plagiogneiss sample HT50-3

Based on the cathodeluminescence (CL) images, zircon grains from the sample HT50-3 show very complex internal structures, such as core–rim or core–mantle–rim structures (Fig. 5a). Zircon grains from this sample are euhedral to subhedral. They are mostly ~100 to 200 μm long, with length to width ratios of 1.5:1–2:1. The cores show oscillatory or patchy zoning, characterized by dully luminescent, indicating that they are likely magmatic zircons modified by subsequent varying degrees metamorphic recrystallization (Hoskin and Black, 2000). The rims are irregular in sharp with relatively bright, homogenous luminescence, suggesting the metamorphic origins (Ayers et al., 2003). Some zircon grains have subhedral-anhedral shape, narrow rim, and do not show any inner structures. These zircon grains show high to moderate luminescent, or dull luminescent. They are mostly metamorphic zircons (Fig. 5a).

One hundred analyses were obtained from 82 zircon grains, and the results are presented on U–Pb Concordia plot (Fig. 6a).

Three zircons have Th/U ratios of 0.21–0.41 (Table 2) and varying apparent $^{207}Pb/^{206}Pb$ age of 2287 ± 19 Ma (spot 50), 2437 ± 18 Ma (spot 27) and 2456 ± 24 Ma (spot 1) (Fig. 6a), they are considered to be inherited or xenocrystic magmatic zircons.

Fifty-three analyses were collected on the magmatic zircon domains, yielding U and Th contents of 20–1030 ppm and 7–990 ppm, respectively, with Th/U ratios of 0.12–0.96 (mostly > 0.3). On the U–Pb Concordia diagram, they plotted along the concordia curve with measured $^{207}Pb/^{206}Pb$ dates ranging from 2390 to 2031 Ma (Fig. 6a). These features indicate variable non-zero radiogenic Pb loss during later metamorphic events. Among them, 24 analyses from a coherent population with a weighted mean $^{207}Pb/^{206}Pb$ age of 2290 ± 11 Ma(MSWD = 1.7), which is interpreted as the magmatic crystallization age of this rock.

Please cite this article in press as: Wu, S., et al. Petrography and zircon U–Pb isotopic study of the Bayanwulashan Complex: Constrains on the Paleoproterozoic evolution of the Alxa Block, westernmost North China Craton. Journal of Asian Earth Sciences (2014), http://dx.doi.org/10.1016/j.jseaes.2014.05.011

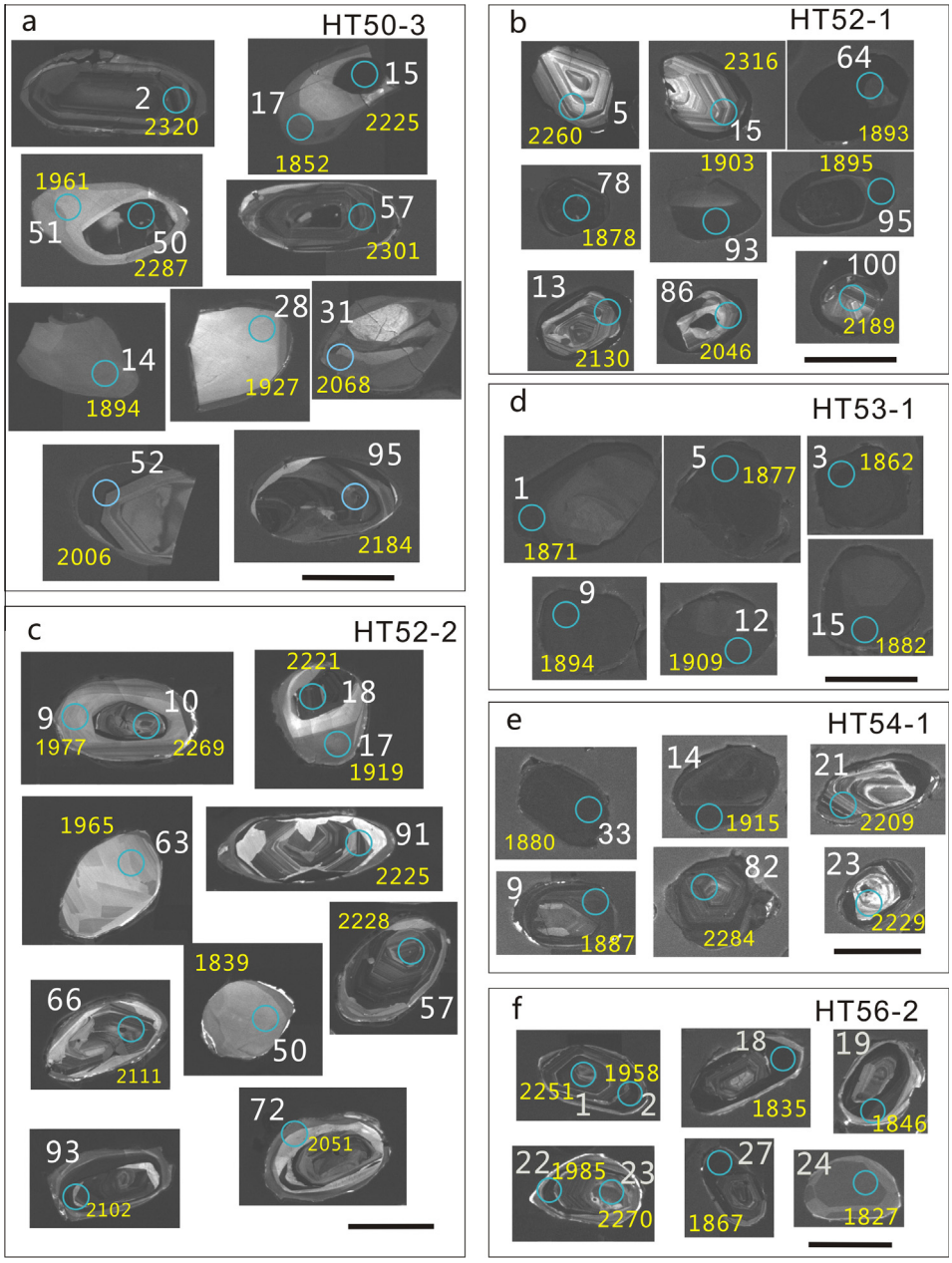

Fig. 5. Cathodoluminescence images of representative zircons for analysis of U–Pb. (a) Sample HT50-3; (b) sample HT52-1; (c): sample HT52-2; (d) sample TH53-1; (e) sample HT54-1; and (f) HT56-2.

Forty-four analyses from the metamorphic zircon domains, including single metamorphic grains and metamorphic rims, yielded $^{207}Pb/^{206}Pb$ dates from 2235 to 1836 Ma, and fourteen analyses have a weighted mean $^{207}Pb/^{206}Pb$ age of 1878 ± 13 Ma (MSWD = 0.69). The age, 1878 ± 13 Ma, is interpreted as the timing of peak metamorphic event of this area.

The ages of 2290 ± 11 Ma and 1878 ± 13 Ma are interpreted as the timing of crystallization and later metamorphism of this sample, respectively. Other analyses plotting along the concordia curve between 2211 and 2031 Ma are interpreted as either incomplete radiogenic Pb loss during the metamorphic event at 1878 Ma, or mixtures between the magmatic and metamorphic domains.

6.2. Granitic gneiss sample HT52-1

Zircon grains from this sample are mostly euhedral to subhedral; a few zircons are in oval shape, and ~100 to 150 μm long with length to width ratios of 1.5:1–2:1 (Fig. 5b). Some zircon grains have subhedral to euhedral crystals and core–rim structures. Most of them are moderate-high luminescent with oscillatory zoning and surrounded by narrow, dull luminescent, structureless rims under CL (Fig. 5b). Few of them have a dull luminescent-zoned core surrounded by dark rim. They are interpreted as magmatic zircons with metamorphic overgrowth. Some zircon grains have subhedral crystals without inner structures. These zircon grains are dull luminescent with or without dark rim. They are mostly metamorphic zircons.

One hundred analyses were obtained from 91 grains. The results are plotted on a U–Pb Concordia diagram (Fig. 6b). They have U and Th contents ranging from 96 to 1519 ppm, and 47 to 1549 ppm, respectively, with Th/U ratios of 0.07–4.21.

Forty-four analyses from the magmatic domain show U and Th contents ranging from 96 to 675 ppm, and 48 to 1549 ppm, respectively, with Th/U ratios of 0.32–4.21 (mostly 0.46–1.2). On

Please cite this article in press as: Wu, S., et al. Petrography and zircon U–Pb isotopic study of the Bayanwulashan Complex: Constrains on the Paleoproterozoic evolution of the Alxa Block, westernmost North China Craton. Journal of Asian Earth Sciences (2014), http://dx.doi.org/10.1016/j.jseaes.2014.05.011

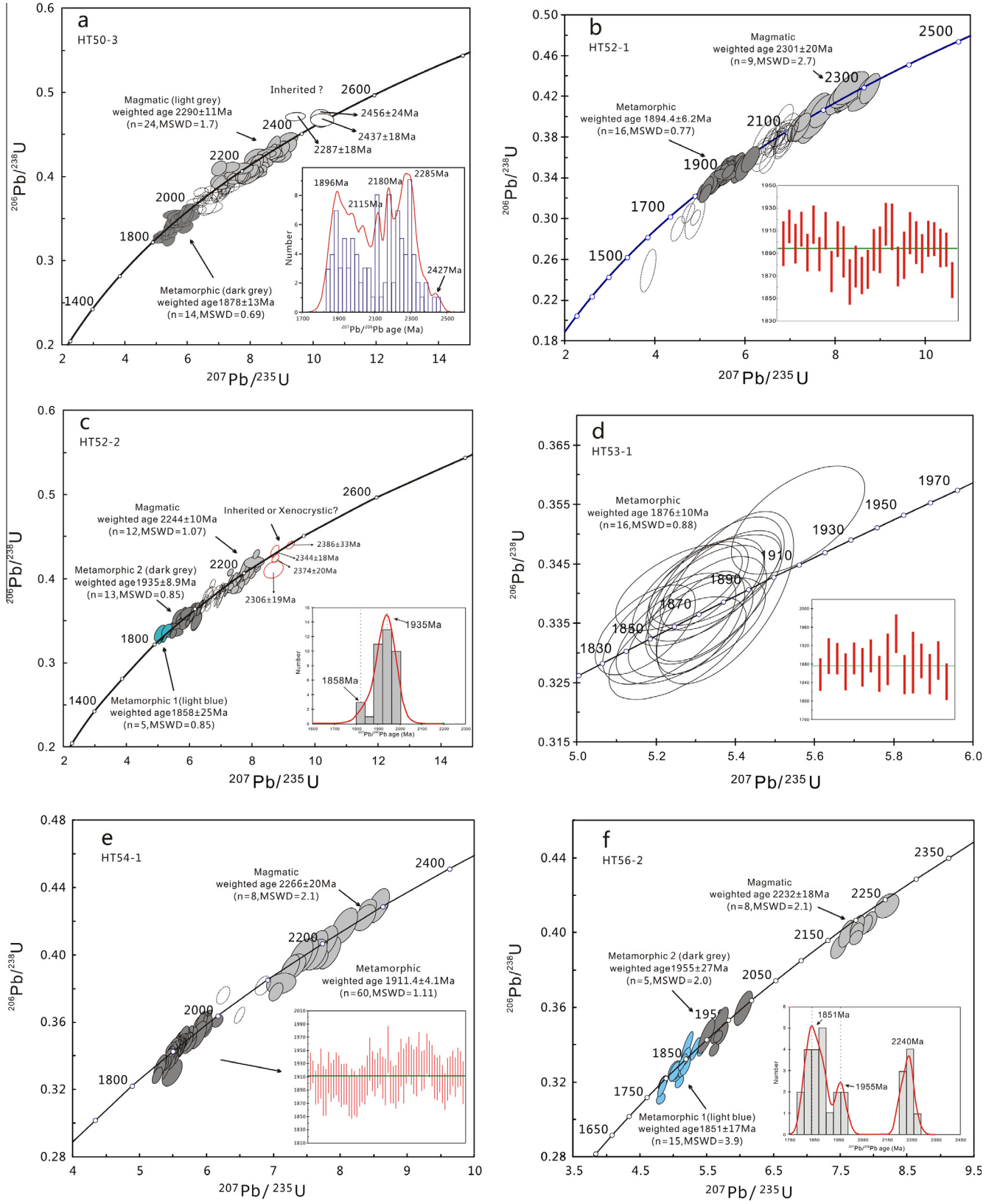

Fig. 6. Condordia diagram of LA-ICP-MS U–Pb zircon data from the Bayanwulashan Complex. (a) Amphibole plagioclase gneiss sample HT50-3; (b) granitic gneiss sample HT52-1; (c) amphibole plagioclase gneiss sample HT52-2; (d) biotite plagioclase gneiss sample HT53-1; (e) biotite plagioclase gneiss sample HT54-1, and (f) monzonite gneiss HT56-2.

Please cite this article in press as: Wu, S., et al. Petrography and zircon U–Pb isotopic study of the Bayanwulashan Complex: Constrains on the Paleoproterozoic evolution of the Alxa Block, westernmost North China Craton. Journal of Asian Earth Sciences (2014), http://dx.doi.org/10.1016/j.jseaes.2014.05.011

the U–Pb Concordia diagram, most of them plotted along the concordia curve with measured $^{207}Pb/^{206}Pb$ ages from 2343 to 1832 Ma, indicating variable non-zero radiogenic Pb loss during the later metamorphic events (Fig. 5b).

Nine analyses yielded consistent $^{207}Pb/^{206}Pb$ dates between 2343 and 2264 Ma, with weight mean of 2301 ± 20 Ma (MSWD = 2.7). This age is interpreted as the crystallization age of this rock.

Fifty-six analyses were conducted on the metamorphic zircon domains, including single metamorphic grains and metamorphic rims. All analyses have U and Th contents ranging from 261 to 1519 ppm and 71 to 1050 ppm, respectively, with Th/U ratios of 0.07–1.09 (mostly ranging from 0.07 to 0.39, except five analyses). On the U–Pb Concordia diagram, most of the analyses plotted along the concordia curve with measured $^{207}Pb/^{206}Pb$ ages from 2124 to 1832 Ma (Fig. 6b). The presence of discordant points below the concordia curve may have been resulted from the Pb loss. Fifty analyses on the metamorphic zircon domains defined a concordia line with an upper intercept age of 1907 ± 13 Ma (MSWD = 1.15), consistent with a weighted mean $^{207}Pb/^{206}Pb$ age of 1904.8 ± 6.0 Ma (MSWD = 0.92) yielded from the thirty-two most concordant data-points (Fig. 6b). The age of 1904.8 ± 6 Ma is interpreted as the peak metamorphic age.

6.3. Amphibole plagiogneiss sample HT52-2

Zircon grains from this sample are mostly euhedral to subhedral; a few zircons are oval in shape. They are mostly elongated, prismatic crystals with pyramidal facets (Fig. 5c), and approximately 100–150 μm long with length to width ratios of 1.5:1–2:1, respectively. Majority of the zircon grains have subhedral to euhedral crystals and core–rim structures. Based on CL images, most of them are dull to moderate luminescent, with clear or fuzzy oscillatory zoning, and surrounded by narrow, moderate to high luminescent structure-less rims. The inner cores and narrow rims are interpreted as magmatic zircons and metamorphic overgrowth, respectively (Fig. 5c). A quarter of the zircon grains have subhedral crystals without inner structures. These zircon grains show moderate to high luminescent, with or without narrow, high luminescent rim (Fig. 5c). They are mostly metamorphic zircons.

One hundred analyses were obtained from 80 grains. The results were plotted on a U–Pb Concordia plot (Fig. 6c). They have U and Th contents ranging from 20 to 686 ppm, and 18 to 359 ppm, respectively, with Th/U ratios of 0.03–3.91. The results are presented in Table 2 and their concordia diagram is shown in Fig. 5b.

Four analyses on the zoned core are independent of other analyses (Fig. 6c) and given $^{207}Pb/^{206}Pb$ ages of 2306 ± 19 Ma (spot 89), 2344 ± 18 Ma (spot 100), 2374 ± 20 Ma (spot 92) and 2386 ± 33 Ma (Spot 96). They are interpreted as inherited or xenocrystic magmatic zircons.

Forty-nine analyses were collected from the magmatic cores. They have U and Th contents ranging from 31 to 532 ppm and 18 to 359 ppm, respectively, with Th/U ratios of 0.28–1.23 (mostly 0.4–1.23 except two analyses). On the U–Pb Concordia diagram, they plotted along the concordia curve with measured $^{207}Pb/^{206}Pb$ ages ranging from 2276 to 1999 Ma (Fig. 6c). This result indicates variable non-zero radiogenic Pb loss during later metamorphic events. Twelve of the 49 analyses with $^{207}Pb/^{206}Pb$ ages ranging from 2276 to 2221 Ma yielded a weighted mean of 2244 ± 10 Ma (MSWD = 1.07), which is interpreted as the crystallization age of this rock.

Forty-seven analyses are from the metamorphic zircon domains, including non-zoning metamorphic grains and metamorphic rims. These analyses can be divided into three groups. Among them, five analyses have a weight mean $^{207}Pb/^{206}Pb$ age of 1858 ± 25 Ma (MSWD = 0.85), and twenty-nine analyses have a $^{207}Pb/^{206}Pb$ age of 1935 ± 8.9 Ma (MSWD = 0.85). These two ages are interpreted to be the timing of two metamorphic events. The remaining 13 analyses from the metamorphic rims gave $^{207}Pb/^{206}Pb$ dates from 2222 to 1980 Ma, which are likely a "mixing age" of the magmatic and metamorphic zircon domains because the rims are mostly narrow, or are chronologically meaningless ages because the zircon U–Th–Pb system had been partially reset during the high-grade metamorphism (see discussion at 7.2).

6.4. Biotite plagioclase gneiss HT53-1

Zircon grains are mostly around 100–150 μm long, with length to width ratios of 1.5:1–1.2:1, respectively. Zircon grains have subhedral-anhedral crystals. Compared with the previous three samples, zircons from HT53-1 have better-developed metamorphic domains that are quite dark in CL, with some showing no inner structures and the others having a dull luminescent zoned core surrounded by dark rim (Fig. 5d). They are mostly metamorphic zircons. Sixteen spots were analyzed on 16 zircons and the results are listed in Table 2. They have U and Th contents ranging from 297 to 793 ppm, and 163 to 328 ppm, respectively, with Th/U ratios of 0.40–0.85. The high Th/U ratios match with the common features of zircons formed at high-grade metamorphic conditions, which have been observed in numerous previous studies of granulite-facies zircons (Kinny, 1986; Grant et al., 2009; Santosh et al., 2009; Wan et al., 2009, 2011a; Zhao, 2009). On the U–Pb Concordia diagram, all the analyses plotted along the concordia curve with measured $^{207}Pb/^{206}Pb$ ages from 1915 to 1862 Ma (Fig. 6d) and define a weighted mean $^{207}Pb/^{206}Pb$ age of 1876 ± 10 Ma (n = 16, MSWD = 0.88), interpreted as the metamorphic age of this rock.

6.5. Biotite plagioclase gneiss HT54-1

Zircon grains show complex structures, most grains have elliptical shape and have either two or three clearly defined domains (core–rim or core–mantle–rim structures). All cores show oscillatory or patchy zoning characterized by high-moderate luminescent, indicating that they are likely magmatic zircons modified by subsequent metamorphic recrystallization to varying degrees. Parts of zircon grains do not show any inner structures. These zircon grains show dull luminescent with or without the dark luminescent rim. They are mostly metamorphic zircons. Eighty-eight analyses were obtained from 85 grains and the results are listed in Table 2.

Nineteen analyses on cores have U contents and Th contents ranging from 158 to 685 ppm, and 104 to 782 ppm, respectively, with Th/U ratios of 0.34–1.14 (mostly > 0.40, except spot 77). On the U–Pb Concordia diagram (Fig. 5e), most of them plotted along the concordia curve with measured $^{207}Pb/^{206}Pb$ ages from 2291 to 2100 Ma (Fig. 6e). Among them, eight analyses lying on or near concordia yield a $^{207}Pb/^{206}Pb$ weighted mean age of 2266 ± 20 Ma (MSWD = 2.1). This age is interpreted as the crystallization age of this rock.

Sixty-nine analyses were collected from the metamorphic zircon domains, including single metamorphic grains and metamorphic rims. All analyses have U and Th contents ranging from 101 to 1838 ppm and 62 to 392 ppm, respectively, with Th/U ratios of 0.07–0.65 (mostly ranging from 0.07 to 0.37, except spot 28). On the U–Pb Concordia diagram, most of the analyses plotted along the concordia curve with measured $^{207}Pb/^{206}Pb$ ages from 2088 to 1880 Ma (Fig. 6e). Sixty ages from the 69 analyses with $^{207}Pb/^{206}Pb$ ages ranging from 1951 to 1880 Ma yielded a weighted mean $^{207}Pb/^{206}Pb$ age of 1911.4 ± 4.1 Ma (MSWD = 1.11), which is interpreted as metamorphic age of this rock.

Please cite this article in press as: Wu, S., et al. Petrography and zircon U–Pb isotopic study of the Bayanwulashan Complex: Constrains on the Paleoproterozoic evolution of the Alxa Block, westernmost North China Craton. Journal of Asian Earth Sciences (2014), http://dx.doi.org/10.1016/j.jseaes.2014.05.011

6.6. Monzonite gneiss HT56–2

Zircon grains from this sample have subhedral to euhedral crystals and core–rim or core–mantle–rim structures. Most of them are with moderate-high luminescent oscillatory zoning core, dull luminescent mantel and surrounded by narrow high-luminescent rims under CL (Fig. 5f). They are interpreted as magmatic zircons with metamorphic overgrowth. Few of them have a dull luminescent structureless core surrounded by dull-moderate luminescent rim. They are mostly metamorphic zircons.

A total of twenty-eight analyses were performed on 25 zircon grains. Eight analyses on cores yielded U and Th contents ranging from 182 to 518 ppm and 165 to 597 ppm, respectively, with Th/U ratios of 0.72–1.18. On the U–Pb Concordia diagram, they plotted along the concordia curve with measured $^{207}Pb/^{206}Pb$ ages ranging from 2270 to 2201 Ma (Fig. 6f). Among them, eight analyses yield a $^{207}Pb/^{206}Pb$ weighted mean age of 2232 ± 18 Ma (MSWD = 2.1). This age is interpreted as the timing of the crystallization of this rock.

Twenty analyses from the metamorphic zircon domains, including single metamorphic grains and the mantles of zoned grains, yielded U and Th contents ranging from 213 to 1744 ppm and 97 to 440 ppm, respectively, with Th/U ratios of 0.06–0.94 (mostly < 0.4). These analyses can be separated into two groups. Among them, fifteen analyses have a weight mean $^{207}Pb/^{206}Pb$ age of 1851 ± 17 Ma (MSWD = 3.9), and five analyses have a $^{207}Pb/^{206}Pb$ age of 1955 ± 27 Ma (MSWD = 2.0). These two ages are interpreted to be the timing of two metamorphic events which are similar to those in sample HT52-2.

7. Discussion

7.1. Age of the protoliths

The BMC used to be grouped into the Archean basement exposures (GSBGMR, 1989; NMBGMR, 1991). Based on our new LA-ICP-MS U–Pb zircon results, the major rock types within the BMC were formed during the Paleoproterozoic period, not the Archean. For the amphibole plagiogneiss, the protolith crystallization ages of 2290 ± 11 Ma and 2244 ± 10 Ma were obtained from samples HT50-3 and HT52-2, respectively. For the granitic gneiss, HT52-1, the magmatic zircons are dated as 2301 ± 20 Ma, which is identical to the crystallization age of amphibole plagiogneiss protolith. For the biotite plagioclase gneiss, no credible crystallization age was obtained from sample HT53-1 due to strong disturbance by later metamorphic events; but crystallization age of 2266 ± 20 Ma was obtained for sample HT54-1. For the monzonite gneiss, eight concordant analyses yield a weighted $^{207}Pb/^{206}Pb$ age of 2232 ± 18 Ma for sample HT56-2, which is interpreted as the crystallization age of its protolith. It is worth noting that most analyses on magmatic zircon domains are distributed along concordia and almost continuously form 2.35 to 2.02 Ga (Fig. 6). Especially for samples HT50-3, HT52-1and HT52-2, ages show large variation ranges. Two possibilities might exist: (1) some of these analyses between the oldest crystallization age and the metamorphic ages are likely a "mixing age" of two different zircon domains because the cores are small, or (2) the high-grade metamorphism had led to the recrystallization of zircons, resulting in the opening and re-adjusting of the U–Th–Pb isotopic system in the zircons to various degrees, therefore, caused the scattered distribution of age data along concordia (Bomparola et al., 2007; Geisler et al., 2007; Wan et al., 2011a). These zircon grains show different structures in CL structures, such as sectorial, banded, or containing mineral inclusions (Fig. 5, e.g. Spot 31, 95 in sample HT50-3, spot 13, 86, and 100 in sample HT52-1, and Spot 66 and93 in sample HT52-2). Those disturbed ages are chronologically meaningless. This has been observed in some previous studies from other areas of the Alxa Block, such as Diebusige Complex (Geng et al., 2010) and Longshoushan Group (Gong et al., 2011), which were interpreted as the resulted from the earlier granulite facies metamorphism.

Thus, the BMC were most likely formed at ca. 2.30–2.23 Ga. Compilation of the previous dating results from BMC indicates that the protoliths were predominantly formed at ca. 2.34–2.27 Ga (Geng et al., 2006a; Dong et al., 2007; Dan et al., 2012a), with a few magmatic zircon ages younger than ca. 2.2 Ga (Li et al., 2004a, 2004b). All of the current magmatic zircons data suggest an Early Paleoproterozoic crustal growth for Alxa complex rather than an Archean crust. The summarized radiometric ages are shown schematically in Fig. 7a.

It worth to note that the majority chronology work from Longshoushan Complex in the southwestern Alxa Block were distributed with in the 2.1–1.9 Ga range (Xiu et al., 2002, 2004; Tung et al., 2007; Gong et al., 2011). However, Gong et al. (2012) and Zhang et al. (2013) have reported the ca.2.5 Ga TTG rock outcropped in the Beidashan area, the western Alxa Block. This may indict a difference between the east and west Alxa Block.

The Diebusige Complex is located in the northeastern Alxa Block. Previous works have grouped the Diebusige Complex as the oldest suite within the traditional Alxa (Huo et al., 1987; NMBGMR, 1991) and suggested that the Diebusige Complex might have formed during Archean (Geng et al., 2007, 2010). However, the recent zircon U–Pb dating of K-feldspar granite and mafic gneiss from Diebusige Complex only identified a few Archean and Paleoproterozoic xenocrystic zircon (Dan et al., 2012a). These isolated U–Pb zircon age points are not enough to support the existence of Archean terrain in the eastern Alxa Block.

All the available radiometric ages are shown schematically in Fig. 7b. There are still a lot of controversies about whether the Archean metamorphic terrains exist in the Alxa Block, but up to present, there is no robust chronological evidence to conclude the existence of the Archean metamorphic events in the eastern part of Alxa Block. Further investigations are needed to answer this question.

7.2. The late Paleoproterozoic metamorphic events

The thermal evolution of a metamorphic body is one of the most important parameters to understanding the tectonic history of the complicated metamorphic terrains (England and Thompson, 1984; Thompson and England, 1984; Harley, 1985, 1989; Bohlen, 1987, 1991; Mengel and Rivers, 1991; Mezger et al., 1991; Brown, 1993). The metamorphic grade of BMC has been classified as upper-amphibolite facies (Shen et al., 2004) or amphibolites facies (Geng et al., 2006a). Multiple stage metamorphisms have been identified within BMC based on the mineral assemblage of plagioclase and amphibole, the chemical variations of amphiboles, and the replacement of amphibole by chlorite and epidote (Fig. 4). The amphiboles from a single rock sample can show significantly different chemical compositions and shapes (Table 1, Fig. 4); indicating that the amphiboles formed under different metamorphic events during late Paleoproterozoic. On the other hand, the patched shapes and the Mn diffusion pattern in garnets also illustrate a retrograde metamorphism after a peak metamorphic episode. Thus, we speculate that the BMC underwent retrograde metamorphic episodes from amphibolites facies to greenschist facies and overprinted the preexisting petrogenesis information.

The amphibole plagiogneiss sample HT52-2 contains two generations of metamorphic zircons dated at 1858 ± 25 Ma and 1935 ± 8.9 Ma. The metamorphic zircon grains and overgrowths from the amphibole plagiogneiss sample HT50-3 are dated at

Please cite this article in press as: Wu, S., et al. Petrography and zircon U–Pb isotopic study of the Bayanwulashan Complex: Constrains on the Paleoproterozoic evolution of the Alxa Block, westernmost North China Craton. Journal of Asian Earth Sciences (2014), http://dx.doi.org/10.1016/j.jseaes.2014.05.011

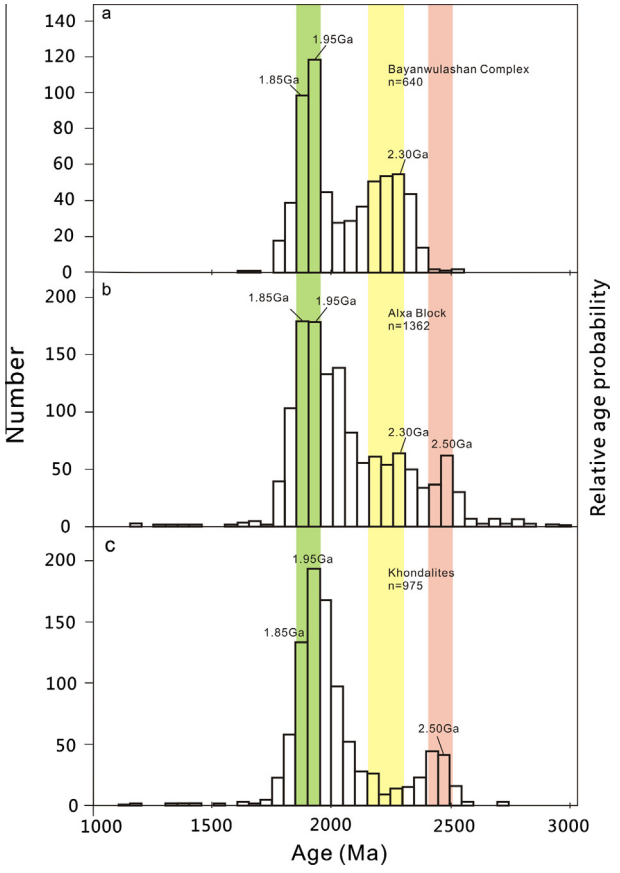

Fig. 7. Compilation of the previous dating results of zircon ages from the Bayanwulashan Complex (a), data sources: this study; Dan et al., 2012a; Dong et al., 2007; Geng et al., 2007; Li et al., 2004a, 2004b), Alxa Block basement (b), data sources: this study; Dan et al., 2012a; Dong et al., 2007; Geng et al., 2007, 2010;Gong et al.,2011,2012; Li et al., 2004a, 2004b; Xiu et al., 2002, 2004; Zhou et al., 2007; Zhang et al.,2013a, 2013b), the Knondalites from Khondalite Belt (c), data sources: Dan et al., 2012b; Dong et al., 2007, 2013; Santosh et al., 2006, 2007a, 2007b; Wan et al., 2013; Xia et al., 2006a, 2006b; Yin et al., 2009; Zhou and Geng, 2009).

1878 ± 13 Ma, which is interpreted to be the second metamorphic event. The granitic gneiss sample HT52-1 recoded the metamorphic event at 1904.8 ± 6.0 Ma. The biotite plagioclase gneiss samples yielded weighted mean $^{207}Pb/^{206}Pb$ age of 1876 ± 10 Ma and 1911.4 ± 4.1 Ma from samples HT53-1 and HT54-1, respectively. The sample HT56-2 contains two generations of metamorphic zircons dated at 1851 ± 17 Ma and 1955 ± 27 Ma, these two ages are interpreted to be the timing of two metamorphic events, which are similar to those in sample HT52-2. The metamorphic ages of some samples vary continuously (Fig. 6) along the concordia curve and cannot be divided into different stages such as sample HT52-2, HT56-2 and previously work (Dong et al., 2007; Dan et al., 2012a). This may be partly due to that high-grade metamorphism had caused recrystallization of early magmatic zircons and formed new zircons, and both of them might be changed during the later metamorphism. The Paleoproterozoic tectonic events had reset the U–Pb system and led to the scattered distribution of U–Pb ages near concordia curve. In this study, magmatic zircons show clear recrystallization features and the metamorphic rims present different structures shown in CL patterns (Fig. 5). Even there are some outliers for the ages of metamorphic zircon; the mode from all ages can still reflect the different metamorphism stages of BMC during the late Paleoproterozoic.

Overall, the BMC underwent two metamorphic events at ca. 1.88–1.86 Ga and ca. 1.95–1.91 Ga. Corresponding with the petrological observations, the older and younger metamorphic ages most likely correspond to the amphibolite facies and greenschist facies metamorphism, respectively. Our results are comparable with the previous reported metamorphic ages of ca.1.92 Ga and ca. 1.86 Ga dated by SHRIMP U–Pb zircon analyses from a quartzofeldspathic gneiss sample (Dong et al., 2007). But our results differ from ca.1.89 Ga and ca. 1.79 Ga dated by SIMS U–Pb zircon analyses for paragneiss, orthogneiss, and mafic samples (Dan et al., 2012a). Dan et al. (2012a) pointed out that this difference might be caused by the different test methods from SIMS. In Diebusige Complex, the northern portion of the Alxa Block, the metamorphic ages can also be grouped into 1.93–1.80 Ga (Geng et al., 2007, 2010), 1.84 Ga and 1.79 Ga (Dan et al., 2012a). In the Longshoushan Complex, the southern part of the Alxa Block, metamorphic ages of ca. 1.93–1.85 Ga have also been recorded (Gong et al., 2011; Lu et al., 2002). Therefore, these different parts of Alxa Block show similar late Paleoproterozoic geological evolution (Fig. 7b). In Khondalite Belt, magmatic ages of ~1.95 Ga and ~1.85 Ga have also been recorded in metamorphic rocks (Fig. 7c).

7.3. Tectonic implications

Controversy exists as to the relationship between the NCC and Alxa Block. Several authors pointed out that the Alxa Block has constituted the western extension of Yinshan Block (Zhao et al., 2005; Zhao, 2009) and some others thought it was part of the Khondalite Belt (Dong et al., 2007; Geng et al., 2010; Gong et al., 2012; Zhang et al., 2013a, 2013b). The ~2.5 Ga magmatic-metamorphic event and subsequent late Paleoproterozoic high-grade metamorphism in Yinshan Block do show similarity to those events of the NCC. However, the tectonic features of the Alxa block indicate that it could evolve separately from the other units of the NCC. Our research have provided the following evidences: (1) the Khondalite Belt consists mainly of khondalite suite and S-type granites and the Yinshan Block are dominated with TTG gneisses in the Guyang area (Zhao et al., 1999, 2005), all these rock units are excessively different from the rock assemblages of the eastern Alxa Block; (2) the ultrahigh temperature (UHT) metamorphic mineral assemblages in the Khondalite Belt (Santosh et al., 2006,2012; Guo et al., 2012), represented by sapphirine granulites in the Daqingshan Complex (Guo et al., 2012) and Jining Complex (Santosh et al., 2007b), have not been reported in the Alxa Block till now; (3) the magmatic activities recorded in BMC are mainly ranged at 2.34–2.27 Ga, which is much younger than the Archean basement rocks in the Khondalite Belt and the eastern Yinshan Block (Zhao et al., 1999; Jian et al., 2005; Zhang et al., 2006). Even the ~2.3 Ga geothermal events have also been reported within the NCC (Zhao et al., 2005; Zhao, 2009; Geng et al., 2006b), the peak magmatic and metamorphic episodes were clearly different from the BMC.

Recent studies have revealed that the Alxa Block and the NCC were the independent blocks prior Early Paleozoic (Li et al., 2012a, 2012b; Zhang et al., 2012, 2013a, 2013b; Yuan and Yang, 2013). These altercating interpretations are mainly based on the following observations: (1) The detrital zircons U–Pb age spectra from Precambrian to Late Mesozoic strata in the western NCC typically have of two age populations at 2.4–2.6 and 1.85–2.1 Ga (Zheng et al., 2004, 2009; Darby and Gehrels, 2006; Xia et al., 2006a, 2006b; He et al., 2009; Jiang et al., 2010; Diwu et al., 2011; Peng et al., 2011; Wan et al., 2011b, 2011c; Yin et al., 2011; Ying et al., 2011; Zhang et al., 2011, 2012) which are similar to those from Neoproterozoic to Early Paleozoic sedimentary rocks in the Zhuozishan Mountains, northwestern Ordos Basin of the NCC (Darby and Gehrels, 2006). However, the U–Pb age spectra obtained from the Middle to Late Devonian sedimentary rocks from the Niushoushan Mountains, located at the southeastern margin of the Alxa

Please cite this article in press as: Wu, S., et al. Petrography and zircon U–Pb isotopic study of the Bayanwulashan Complex: Constrains on the Paleoproterozoic evolution of the Alxa Block, westernmost North China Craton. Journal of Asian Earth Sciences (2014), http://dx.doi.org/10.1016/j.jseaes.2014.05.011

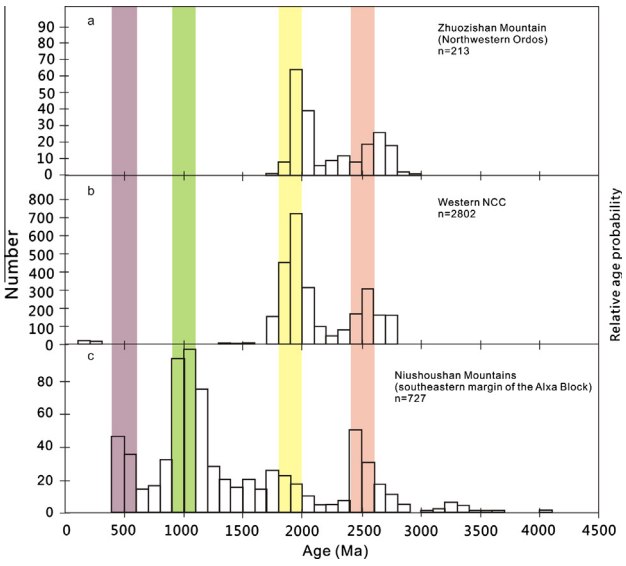

Fig. 8. Relative age probability plot comparing the ages of setrital zircons from the Zhuozishan Mountains adjacent to the western margin of Ordos Basin in the NCC (a), data after: Darby and Gehrels, 2006);the western NCC (b), data after: Zheng et al., 2004; Darby and Gehrels, 2006; Xia et al., 2006a, 2006b;He et al., 2009; Zheng et al., 2009; Jiang et al., 2010; Diwu et al., 2011; Peng et al., 2011;Wan et al., 2011b, 2011c; Yin et al., 2011; Ying et al., 2011; Zhang et al., 2012; Zhang et al., 2011) and the Alxa Block (c), data after: Zhang et al.,2012; Yuan and Yang, 2013).

Block, yielded significant different age populations compared with those in the NCC (Zhang et al., 2012; Yuan and Yang, 2013) (Fig. 8); (2) field geological observations and ductile deformation measurements demonstrate the different stress field between eastern Alxa Block and the NCC prior the end of the Devonian (Li et al.,2012a, 2012b; Zhang et al.,2013a, 2013b); and (3) the paleomagnetic results can only conclude that Alxa Block had combined with NNC as its western extension by either Late Cambrian time (Meng et al., 1990; Wu et al., 1993; Huang et al.,1999, 2000, 2001) or after the Early to Middle Triassic (Liu et al., 2010a, 2010b) or before Early Cretaceous (Yuan and Yang, 2014).

Our new study for BMC recorded a gradual transition from amphibole to greenschist facies metamorphism and the metamorphic zircons show a continuous age span with two peaks at ca. 1.94 and 1.86 Ga. The earlier metamorphic event at ca. 1.94–1.91 Ga was stronger than the younger event at ca. 1.88–1.86 Ga. The correlated two Paleoproterozoic tectonothermal events has also been observed in the metamorphic basement from different areas of the Alxa Block and the Khondalite Belt (Dong et al., 2007; Geng et al., 2007, 2010; Zhou et al., 2007) (Fig. 7). Even the tectonic model that the NCC formed by the amalgamation of the Eastern and Western Blocks along TNCO is widely accepted, the exact time of this amalgamation is still under considerable debate. The current generally accepted time frames for the plate accretion are as following: the Ordos and Yinshan Blocks amalgamated along the Khondalite Belt and formed the Western Block at ca. 1.95 Ga (Yin et al., 2009; Santosh et al., 2010; Zhao et al., 2010); while the unified NCC was formed by a collision between the Eastern and Western Blocks along the TNCO at ca. 1.85 Ga (Zhao et al., 2004; Santosh et al., 2007b, 2010). The east margin of Alxa Block should have been affected by the ca. 1.95 Ga and ca. 1.85 Ga juxtaposition of NCC.

In summary, the Early Paleoproterozoic tectonothermal characters in the Alxa Block are different from the Khondalite Belt and Ordos Block. This suggests that Alxa Block is most likely an independent terrain during Early Paleoproterozoic. Following the Late Paleoproterozoic accretionary and collisional events, the Alxa Block joined the NCC with the final amalgamation at ca. 1.85 Ga.

8. Conclusions

1. New LA-ICP-MS U–Pb zircon analyses from the BMC reveal magmatic crystallization ages of ca. 2.30–2.24 Ga, suggesting that the Bayanwulashan magmatic events occurred at Paleoproterozoic, not Archean.
2. The BMC was subjected to two metamorphic events at ca. 1.94–1.91 Ga and ca. 1.88–1.86 Ga. These metamorphic ages were corresponding to the late Paleoproterozoic tectonothermal events during the final amalgamation of NCC.

Acknowledgments

We thank Shuanhong Zhang, Wei Wang, and Xiaochun Liu for their useful and helpful suggestions, Jianzhen Geng from the MC-LA-ICP-MS Lab of Tianjin Institute of Geology and Mineral Resources for his help in LA–MC–ICP-MS analyses. Comments from anonymous reviewers and journal editor have greatly improved this manuscript. This research was funded by the National Basic Research Program of China (2012CB416604) and the National Natural Science Foundation of China (91114204).

Appendix A. Supplementary material

Supplementary data associated with this article can be found, in the online version, at http://dx.doi.org/10.1016/j.jseaes.2014.05.011.

References

Andersen, T.B., 2002. Correction of common lead in U–Pb analyses that do not report 204Pb. Chem. Geol. 192, 59–79.
Ayers, J.C., Delacruz, K., Miller, C., Switzer, O., 2003. Experimental study of zircon coarsening in quartzite ±H_2O at 1.0 GPa and 1000 °C, with implications for geochronological studies of high-grade metamorphism. Am. Mineral. 88, 365–376.
Black, L.P., Kamo, S.L., Allen, C.M., Aleinikoff, J.N., Davis, D.W., Korsch, R.J., Foudoulisa, C., 2003. TEMORA 1: a new zircon standard for Phanerozoic U–Pb geochronology. Chem. Geol. 200, 155–170.
Bochez, J., 1977. Plastic deformation of quartites at lower temperature in an area of natural strain gradient. Tectonophiscs 39, 25–50.
Bohlen, S.R., 1987. Pressure-temperature-time paths and a tectonic model for the evolution of granulites. J. Geol., 617–632.
Bohlen, S.R., 1991. On the formation of granulites. J. Metamorph. Geol. 9, 223–229.
Bomparola, R.M., Ghezzo, C., Belousova, E., Griffin, W.L., O'Reilly, S.Y., 2007. Resetting of the UePb zircon system in Cambro-Ordovician intrusives of the deep freeze range, northern Victoria Land, Antarctica. J. Petrol. 48, 327–364.
Brown, M., 1993. P–T–t evolution of orogenic belts and the causes of regional metamorphism. J. Geol. Soc. 150, 227–241.
Dan, W., Li, X.H., Guo, J.H., Liu, Y., Wang, X.C., 2012a. Paleoproterozoic evolution of the eastern Alxa Block, westernmost North China: evidence from in situ zircon U–Pb dating and Hf–O isotopes. Gondwana Res. 21, 838–864.
Dan, W., Li, X.H., Guo, J.H., Liu, Y., Wang, X.C., 2012b. Integrated in situ zircon U–Pb age and Hf–O isotopes for the Helanshan khondalites in North China Craton: juvenile crustal materials deposited in active or passive continental margin? Precambr. Res. 222–223, 143–158.
Darby, B.J., Gehrels, G., 2006. Detrital zircon reference for the North China block. J. Asian Earth Sci. 26, 637–648.
Diwu, C.R., Sun, Y., Guo, A.L., Wang, H.L., Liu, X.M., 2011. Crustal growth in the North China Craton at 2.5 Ga: evidence fromin situzircon U–Pb ages, Hf isotopes and whole-rock geochemistry of the Dengfeng complex. Gondwana Res. 20, 149–170.
Dong, C.Y., Liu, D.Y., Li, J.J., Wan, Y.S., Zhou, H.Y., Li, C.D., Yang, Y.H., Xie, L.W., 2007. Palaeoproterozoic Khondalite Belt in the western North China Craton: new evidence from SHRIMP dating and Hf isotope composition of zircons from metamorphic rocks in the Bayan Ul-Helan Mountains area. Chin. Sci. Bull. 52, 2984–2994.
Dong, C.Y., Wan, Y.S., Wilde, S.A., Xu, Z.Y., Ma, M.Z., Xie, H.Q., Liu, D.Y., 2013. Earliest Paleoproterozoic supracrustal rocks in the North China Craton recognized from the Daqingshan area of the Khondalite Belt: constraints on craton evolution. Gondwana Res., <http://dx.doi.org/10.1016/j.gr.2013.05.02>.
Droop, G.T.R., 1987. A general equation for estimating Fe3+ concentrations in ferromagnesian silicates and oxides from microprobe analyses, using stoichiometric criteria. Mineral Mag. 51, 431–435.

England, P.C., Thompson, A.B., 1984. Pressure-temperature-time paths of regional metamorphism I. Heat transfer during the evolution of regions of thickened continental crust. J. Petrol. 25, 894–928.

Geisler, T., Schaltegger, U., Tomaschek, F., 2007. Re-equilibration of zircon in aqueous fluids and melts. Elements 3, 43–50.

Geng, Y.S., Wang, X.S., Shen, Q.H., Wu, C.M., 2002. The discovery of Neoproterozoic Jinningian deformed granites in Alxa area and its significance. Acta prtrological ET mineralogica 21, 412–420 (in Chinese with English abstract).

Geng, Y.S., Wang, X.S., Shen, Q.H., Wu, C.M., 2006a. Redefinition of the Alxa Group-complex (Precambrian metamorphic basement) in the Alxa area, Inner Mongolia. Geol. China 33, 138–145 (in Chinese with English abstract).

Geng, Y.S., Yang, C.H., Wan, Y.S., 2006b. Paleoproterozoic granitic magmatism in the Lüliang area. North China Craton: constraint from isotopic geochronology. Geol. China 22, 305–314 (in Chinese with English abstract).

Geng, Y.S., Wang, X.S., Shen, Q.H., Wu, C.M., 2007. Chronology of the Precambrian metamorphic series in the Alxa area, Inner Mongolia. Geol. China 34, 251–261 (in Chinese with English abstract).

Geng, Y.S., Wang, X.S., Wu, C.M., Zhou, X.W., 2010. Late-Paleoproterozoic tectonothermal events of the metamorphic basement in Alxa area:Evidence from geochronology. Acta Petrologica Sinica 26, 1159–1170 (in Chinese with English abstract).

Geng, Y.S., Zhou, X.W., 2010. Early Neoproterozoic granite events in Alxa area of InnerMongolia and their geological significance: evidence from geochronology. Acta Petorlogica Et Mineralogica 29, 779–795 (in Chinese with English abstract).

Gong, J.H., Zhang, J.X., Yu, S.Y., 2011. The origin of Longshoushan Group and associated rocks in the southern part of the Alxa block: constraint from LA-ICP-MS U–Pb zircon dating. Acta Pretrologica Et Mineralogica 30, 795–818 (in Chinese with English abstract).

Gong, J.H., Zhang, J.X., Yu, S.Y., Li, H.K., Hou, K.J., 2012. Ca. 2.5 Ga TTG rocks in the western Alxa Block and their implications. Chin. Sci. Bull. 57, 4064–4076.

Grant, M.L., Wilde, S.A., Wu, F.Y., Yang, J., 2009. The application of zircon cathodoluminescence imaging, Th–U–Pb chemistry and U–Pb ages in interpreting discrete magmatic and high-grade metamorphic events in the North China Craton at the Archean/Proterozoic boundary. Chem. Geol. 261 (1), 155–171.

Guo, J.H., Peng, P., Chen, Y., Jiao, S.J., Windley, B.F., 2012. UHT sapphirine granulite metamorphism at 1.93–1.92 Ga caused by gabbronorite intrusions: Implications for tectonic evolution of the northern margin of the North China Craton. Precambr. Res. 222–223, 124–142.

GSBGMR (Gansu Bureau of Geology and Mineral Resources), 1989. Regional Geology of Gansu Province. Geological Publishing House, Beijing, (in Chinese).

Harley, S., 1985. Garnet-orthopyroxene bearing granulites from Enderby Land, Antarctica: metamorphic pressure temperature-time evolution of the Archaean Napier Complex. J. Petrol. 26, 819–856.

Harley, S.L., 1989. The origins of granulites: a metamorphic perspective. Geol. Mag. 126, 215–247.

He, Y.H., Zhao, G.C., Sun, M., Xia, X.P., 2009. SHRIMP and LA–ICP–MS zircon geochronology of the Xiong'er volcanic rocks: implications forthe Paleo-Mesoproterozoic evolution of the southern margin of the North China Craton. Precambr. Res. 168, 213–222.

Hippertt, J., Rocha, A., Lana, C., Silva, E., Takeshita, T., 2001. Quartz plastic segregation and ribbon in high-grade striped gneisses. J. Struct. Geol. 23, 67–80.

Hoskin, P.W.O., Black, L.P., 2000. Metamorphic zircon formation by solid-state recrystallization of protolith igneous zircon. J. Metamorph. Geol. 18, 423–439.

Huang, B.C., Yang, Z.Y., Otofuji, Y., Zhu, R.X., 1999. Early Paleozoic paleomagnetic poles from the western part of the North China Block and their implications. Tectonophysics 308, 377–402.

Huang, B.C., Otofuji, Y.I., Yang, Z.Y., Zhu, R.X., 2000. New Silurian and Devonian paleomagnetic results from the Hexi Corridor terrane, Northwest China, and their tectonicimplications. Geophys. J. Int. 140, 132–146.

Huang, B.C., Otofuji, Y.I., Zhu, R.X., Shi, R.P., Wang, Y.C., 2001. Paleomagnetism of Carboniferous sediments in the Hexi corridor: its origin and tectonic implication. Earth Planet. Sci. Lett. 194, 135–149.

Huo, F.C., Cao, J.X., Dong, Y.S., Gu, Q.C., Yan, Z.Q., 1987. The division, correlation, metamorphism and mineralization features of the lower and middle Precambrian in the Helanshan Moutain-Alashan Region, China. J. Changchun Coll. Geol. 17 (1), 35–46.

Jackson, S.E., Pearson, N.J., Griffin, W.L., Belousova, E.A., 2004. The application of laser ablation-inductively coupled plasma-mass spectrometry to in situ U–Pb zircon geochronology. Chem. Geol. 211 (1), 47–69.

Jian, P., Zhang, Q., Liu, D.Y., Jin, W.J., Jia, X.Q., Qian, Q., 2005. SHRIMP dating and geological significance of Late Achaean high-Mg diorite (sanukite) and hornblende-granite at Guyang of Inner Mongolia. Acta Petrological Sinica 21, 151–157.

Jiang, N., Guo, J.H., Zhai, M.G., Zhang, S.Q., 2010. ~2.7 Ga crust growth in the North China Craton. Precambr. Res. 179, 37–49.

Kinny, P.D., 1986. 3820 Ma zircons from a tonalitic Amitsoq gneiss in the Goldthab district of southern West Greenland. Earth Planet. Sci. Lett. 79, 337–347.

Kohn, M.J., Spear, F., 2000. Retrograde net transfer reaction insurance for pressure-temperature estimates. Geology 28, 1127–1130.

Kröner, A., Wilde, S.A., Li, J.H., Wang, K.Y., 2005. Age and evolution of a late Archean to Paleoproterozoic upper to lower crustal section in the Wutaishan/Hengshan/Fuping terrain of northern China. J. Asian Earth Sci. 24, 577–595.

Leake, B.E., Woolley, A.R., Arps, C.E.S., Birch, W.D., Gilbert, M.C., Grice, J.D., Hawthorne, F.C., Kato, A., Kisch, H.J., Krivovichev, V.G., Linthout, K., Laira, J., Mandarino, J.A., Maresch, W.V., Nickel, E.H., Rock, N.M.S., Schumacher, J.C., Smith, D.C., Steohenson, N.C.N., Ungaretti, L., Whittaker, E.J.W., Guo, Y., 1997. Nomenclature of amphiboles: report of the subcommittee on amphiboles of the International Mineralogical Association, Commission on New Minerals and Mineral Names. Can. Mineral. 35, 219–246.

Leake, B.E., Woolley, A.R., Birch, W.D., Bruke, E.A.J., Ferraris, G., Grice, J.D., 2004. Nomenclature of amphiboles: additions and revisions to the International Mineralogical Association's amphibole nomenclature. Am. Mineral. 89, 883–887.

Li, J.J., Shen, B.F., Li, H.M., Zhou, H.Y., Guo, L.J., Li, C.Y., 2004a. Single-zircon U–Pb age of granodioritic gneiss in the Bayan Ul area, western Inner Mongolis. Geol. Bull. China, 1243–1245.

Li, J.Y., Zhang, J., Qu, J.F., 2012a. Amalagmation of North China Craton with Alxa Block in the Late of Early Paleozoic: Evodengce from sedmentary sequences in the Niushou Mountain, Ningxia Hui Autonomous Region, Nw China. Geol. Rev. 58, 208–214.

Li, S.Z., Zhao, G.C., Liu, X., Dai, L.M., Suo, Y.H., Song, M.C., Wang, P.C., 2012b. Structural evolution of the southern segment of the Jiao–Liao–Ji Belt, North China Craton. Precambr. Res. 200, 59–73.

Li, S.Z., Zhao, G.C., Santosh, M., Liu, X., Dai, L.M., 2011. Palaeoproterozoic Tectono-thermal Evolution and Deep Crustal Processes in the Jiao–Liao–Ji Belt, North China craton: a review. Geol. J. 46, 525–543.

Li, S.Z., Zhao, G.C., Zhang, J., Sun, M., Zhang, G.W., Dai, L.M., 2010. Deformation history of the Hengshan–Wutai–Fuping complexes: implications for the evolution of the Trans-North China Orogen. Gondwana Res. 18, 611–631.

Li, S.Z., Zhao, G.C., 2007. SHRIMP U–Pb zircon geochronology of the Liaoji Granitoids: constraints on the Paleoproterozoic Jiao–Liao–Ji belt in the eastern block of the North China craton. Precambr. Res. 158 (1–2), 1–16.

Li, S.Z., Zhao, G.C., Sun, M., Luo, Y., Han, Z.Z., Zhao, G.T., 2006. Are the South and North Liaohe Groups different exotic terranes?—Nd isotope constraints on the Jiao–Liao–Ji orogen. Gondwana Res. 9, 198–208.

Li, S.Z., Zhao, G.C., Sun, M., Han, Z.Z., Hao, D.f., Luo, Y., Xia, X.P., 2005. history of the Paleoproterozoic Liaohe Group in the Eastern Block of the North China Craton. J. Asian Earth Sci. 24 (5), 659–674.

Li, X.H., Su, L., Song, B., Liu, D.Y., 2004b. SHRIMP U–Pb zircon age of the Jinchuan ultramafic intrusion and its geological significance. Chin. Sci. Bull. 49, 401–402.

Liu, J., Yang, Z.Y., Tong, Y.B., Yuan, W., 2010a. Tectonic implications of early–middle Triassic palaeomagnetic results from Hexi Corridor, North China. Geophys. J. Int. 182 (3), 1216–1228.

Liu, Y.S., Hu, Z.C., Zong, K.Q., Gao, C.G., Gao, S., Xu, J., Chen, H.H., 2010b. Reappraisement and refinement of zircon U–Pb isotope and trace element analyses by LA-ICP-MS. Chin. Sci. Bull. 55 (15), 1535–1546.

Lu, S.N., Yu, H.F., Ji, W., Li, H.K., Zheng, J.K., 2002. Microcontinents on the eastrn margin of Tarim paleocontinent. Acta Petrologica Et Mineralogica 21, 317–326.

Ludwig, K.R., 2003. User's manual for Isoplot 3.00: A geochronological toolkit for Microsoft Excel. No. 4. Kenneth R. Ludwig, 2003. Berkeley Geochronology Center Special Publication No.4a.

Meng, Z.F., Huang, H.F., Chen, Y.Z., 1990. The late Permian pole of the western Jiuquanbasin (NW China) and its tectonic implication. Acta Sedimentol. Sin. 8 (3), 58–65 (in Chinese with English abstract).

Mengel, F., Rivers, T., 1991. Decompression Reactions and P–T Conditions in High-grade Rocks, Northern Labrador: P–T–t Paths from Individual Samples and Implications for Early Proterozoic Tectonic Evolution. J. Petrol. 32, 139–167.

Mezger, K., Rawnsley, C.M., Bohlen, S.R., Hanson, G.N., 1991. U–Pb garnet, sphene, monazite, and rutile ages: Implications for the duration of high-grade metamorphism and cooling histories, Adirondack Mts., New York. J. Geol., 415–428.

NMBGMR (Nei Mongol Bureau of Geology and Mineral Resources), 1991. Regional Geology of Nei Mongol Autonomous Region. Geological Publishing House, Beijing. (in Chinese).

Peng, P., Guo, J.H., Windley, B.F., Li, X.H., 2011. Halaqin volcano-sedimentary succession in the central-northern margin of the North China Craton: products of Late Paleoproterozoic ridge subduction. Precambr. Res. 187, 165–180.

Ren, J.S., Jiang, C.F., Zhang, Z.K., Qing, D.Y., 1987. Geotectonic Evolution of China. Springer, Berlin.

Santosh, M., Sajeev, K., Li, J.H., 2006. Extreme crustal metamorphism during Columbia supercontinent assembly: evidence from North China Craton. Gondwana Res. 10, 256–266.

Santosh, M., Tsunogae, T., Li, J.H., Liu, S.J., 2007a. Discovery of sapphirine-bearing Mg–Al granulites in the North China Craton: implications for Paleoproterozoic ultrahigh temperature metamorphism. Gondwana Res. 11, 263–285.

Santosh, M., Wilde, S.A., Li, J.H., 2007b. Timing of Paleoproterozoic ultrahigh-temperature metamorphism in the North China Craton: evidence from SHRIMP U–Pb zircon geochronology. Precambr. Res. 159, 178–196.

Santosh, M., Tsunogae, T., Ohyama, H., Sato, K., Li, J.H., Liu, S.J., 2008. Carbonic metamorphism at ultrahigh-temperatures: evidence from North China Craton. Earth Planet. Sci. Lett. 266, 149–165.

Santosh, M., Wan, Y.S., Liu, D.Y., Dong, C.Y., Li, J.H., 2009. Anatomy of zircons from an ultra-hot orogen: the amalgamation of the North China Craton within the supercontinent Columbia. J. Geol. 117, 429–443.

Santosh, M., Zhao, D.P., Kusky, T., 2010. Mantle dynamics of the Paleoproterozoic North China Craton: a perspective based on seismic tomography. J. Geodyn. 49, 39–53.

Santosh, M., Liu, S.J., Tsunogae, T., Li, J.H., 2012. Paleoproterozoic ultrahigh-temperature granulites in the North China Craton: implications for tectonic models on extreme crustal metamorphism. Precambr. Res. 222, 77–106.

Please cite this article in press as: Wu, S., et al. Petrography and zircon U–Pb isotopic study of the Bayanwulashan Complex: Constrains on the Paleoproterozoic evolution of the Alxa Block, westernmost North China Craton. Journal of Asian Earth Sciences (2014), http://dx.doi.org/10.1016/j.jseaes.2014.05.011

Shen, Q.H., Geng, Y.S., Wang, X.S., Wu, C.M., 2004. Mineral characteristics and metamorphic P–T condition of Precambrian amphibolites in Alxa region. Geol. Surv. Res. 27, 209–216 (in Chinese with English abstract).

Shen, Q.H., 2009. The recommendation of a systematic of mineral abbreviations. Acta Petrological et Mineralogica 28 (5), 495–500 (in Chinese with English abstract).

Thompson, A.B., England, P.C., 1984. Pressure—Temperature—Time Paths of Regional Metamorphism II. Their Inference and Interpretation using Mineral Assemblages in Metamorphic Rocks. J. Petrol. 25, 929–955.

Tung, K.A., Yang, H.Y., Liu, D.Y., Zhang, J.X., Tseng, C.Y., Wan, Y.S., 2007. SHRIMP U–Pb geochronology of the detrital zircons from the Longshoushan Group and its tectonic significance. Chin. Sci. Bull. 52, 141–1425.

Wan, Y.S., Song, B., Liu, D.Y., Wilde, S.A., Wu, J.S., Shi, Y.R., Yin, X.Y., Zhou, H.Y., 2006. SHRIMP U–Pb zircon geochronology of Palaeoproterozoic metasedimentary rocks in the North China Craton: Evidence for a major Late Palaeoproterozoic tectonothermal event. Precambr. Res. 149, 249–271.

Wan, Y.S., Liu, D.Y., Dong, C.Y., Xu, Z.Y., Wang, Z.J., Wilde, S.A., Yang, Y.H., Liu, Z.H., Zhou, H.Y., 2009. The Precambrian Khondalite Belt in the Daqingshan area, North China Craton: evidence for multiple metamorphic events in the Palaeoproterozoic era. In: Reddy, S.M., Mazumder, R., Evans, D.A.D., Collins, A.S. (Eds.), Palaeoproterozoic Supercontinents and Global Evolution, vol. 323. Geological Society, London, Special Publication, pp. 73–97.

Wan, Y.S., Liu, D.Y., Dong, C.Y., Liu, S.J., Wang, S.J., Yang, E.X., 2011a. U–Th–Pb behavior of zircons under high-grade metamorphic conditions: a case study of zircon dating of meta-diorite near Qixia, eastern Shandong. Geosci. Front. 2 (2), 137–146.

Wan, Y.S., Liu, D.Y., Wang, S.J., Yang, E.X., Wang, W., Dong, C.Y., Zhou, H.Y., Du, L.L., Yang, Y.H., Diwu, C.R., 2011b. Ga juvenile crust formation in the North China Craton (Taishan–Xintai area, western Shandong Province): further evidence of an understated event from U–Pb dating and Hf isotopic composition of zircon. Precambr. Res. 186, 169–180.

Wan, Y.S., Liu, D.Y., Wang, W., Song, T.R., Kroner, A., Dong, C.Y., Zhou, H.Y., Yin, X.Y., 2011c. U–Pb and Hf isotopic study of detrital zircons from the Wulashan khondalites constraints on the evolution of the Ordos Terrane, Western Block of the North China Craton. Gondwana Res. 20, 219–242.

Wan, Y.S., Xu, Z.Y., Dong, C.Y., Nutman, A., Ma, M.Z., Xie, H.Q., Liu, S.J., Liu, D.Y., Wang, H.C., Cu, H., 2013. Episodic Paleoproterozoic (~2.45, ~1.95 and ~1.85 Ga) mafic magmatism and associated high temperature metamorphism in the Daqingshan area, North China Craton: SHRIMP zircon U–Pb dating and whole-rock geochemistry. Precambr. Res. 224, 71–93.

Wilde, S.A., Zhao, G.C., Sun, M., 2002. Development of the North China Craton During the Late Archaean and its Final Amalgamation at 1.8 Ga: some Speculations on its Position Within a Global Palaeoproterozoic Supercontinent. Gondwana Res. 5, 85–94.

Wu, J.S., Geng, Y.S., Shen, Q.H., Wan, Y.S., Liu, D.Y., Song, B., 1998. Archean Geological Characteristics and Tectonic Evolution of China-Korea Paleo-Continent. Geological Publishing House, Beijing (in Chinese).

Wu, H.N., Zhou, L.F., Zhao, Z.Y., 1993. Tectonic implication of the paleomagnetic result of the later Paleozoic and Mesozoic rocks from the Alax area of the western North China block. Sci. Geol. Sinica 2 (1), 19–46 (In Chinese with English abstract).

Wu, M.L., Zhao, G.C., Sun, M., Yin, C.Q., Li, S.Z., Tam, Pui Yuk, 2012. Petrology and P–T path of the Yishui mafic granulites: implications for tectonothermal evolution of the Western Shandong Complex in the Eastern Block of the North China Craton. Precambr. Res. 222, 312–324.

Wu, M.L., Zhao, G.C., Sun, M., Li, S.Z., He, Y.H., Bao, Z., 2013. Zircon U–Pb geochronology and Hf isotopes of major lithologies from the Yishui Terrane: implications for the crustal evolution of the Eastern Block, North China Craton. Lithos 170, 164–178.

Xia, X.P., Sun, M., Zhao, G.C., Luo, Y., 2006a. LA-ICP-MS U–Pb geochronology of detrital zircons from the Jining Complex, North China Craton and its tectonic significance. Precambr. Res. 144, 199–212.

Xia, X.P., Sun, M., Zhao, G.C., Wu, F.Y., Xu, P., Zhang, J.H., Luo, Y., 2006b. U–Pb and Hf isotopic study of detrital zircons from the Wulashan khondalites: Constraints on the evolution of the Ordos Terrane, Western Block of the North China Craton. Earth Planet. Sci. Lett. 241, 581–593 (in Chinese with English abstract).

Xiu, Q.Y., Lu, S.N., Yu, H.F., Yang, C.L., 2002. The Isotopic age Evidence for Main Longshoushan Lroup Contributing to Palaeoproterozoic. Progr. Precambrian Res. 25, 93–96 (in Chinese with English abstract).

Xiu, Q.Y., Yu, H.F., Li, J., Zuo, G.C., Li, J.W., Cao, C.J., 2004. Discussion on the Petrogenic Time of Longshoushan Group, Gansu Province. Acta Geol. Sin.–Chinese Ed. 78, 366–373 (in Chinese with English abstract).

Yin, C.Q., Zhao, G.C., Sun, M., Xia, X.P., Wei, C.J., Zhou, X., Leung, W.H., 2009. LA-ICP-MS U–Pb zircon ages of the Qianlishan Complex: Constrains on the evolution of the Khondalite Belt in the Western Block of the North China Craton. Precambr. Res. 174, 78–94.

Yin, C.Q., Zhao, G.C., Guo, J.H., Sun, M., Xia, X.P., Zhou, X.W., Liu, C.H., 2011. U–Pb and Hf isotopic study of zircons of the Helanshan complex: constrains on the evolution of the Khondalite Belt in the Western Block of the North China Craton. Lithos 122, 25–38.

Ying, J.F., Zhang, H.F., Tang, Y.J., 2011. Crust–mantle interaction in the central North China Craton during the Mesozoic: evidence from zircon U–Pb chronology, Hf isotope and geochemistry of syenitic–monzonitic intrusions from Shanxi province. Lithos 125, 449–462.

Yuan, W., Yang, Z.Y., 2013. The Alashan Terrane was not part of North China by the Late Devonian: evidence from detrital zircon U–Pb geochronology and Hf isotopes. Gondwana Res., <http://dx.doi.org/10.1016/j.gr.2013.12.009>.

Yuan, W., Yang, Z.Y., 2014. Alashan Terrane did not amalgamate with North China block by the Late Permian: evidence from Carboniferous and Permian paleomagnetic results. J. Asian Earth Sci., <http://dx.doi.org/10.1016/j.jseaes.2014.02.010>.

Zhang, J., Li, J.Y., Liu, J.F., Li, Y.F., Qu, J.F., Feng, Q.W., 2012. The relationship between the Alxa block and the North China Plate during the Early Paleozoic: new information from the Middle Ordovician detrital zircon ages in the eastern Alxa Block. Acta Petrological Sinica 28, 2912–2934.

Zhang, J., Li, J.Y., Xiao, W.X., Wang, Y.N., Qi, W.H., 2013. Kinematics and geochronology of multistage ductile deformation along the eastern Alxa block, NW China: new constraints on the relationship between the North China Plate and the Alxa block. J. Struct. Geol., 10.1016/j.jsg.2013.10.002.

Zhang, J.X., Gong, J.H., Yu, S.Y., Li, H.K., Hou, K.J., 2013b. Neoarchean-Paleoproterozoic multiple tectonothermal events in the western Alxa block, North China Craton and their geological implication: Evidence from zircon U–Pb ages and Hf isotopic composition. Precambr. Res. 235, 36–57.

Zhang, X.J., Zhang, L.C., Xiang, P., Wan, B., Pirajno, F., 2011. Zircon U–Pb age, Hf isotopes and geochemistry of Shuichang Algoma-type banded iron-formation, North China Craton: constraints on the ore-forming age and tectonic setting. Gondwana Res. 20, 137–148.

Zhang, Y.Q., Zhang, Y.K., Zheng, B.J., Xu, G.Q., Han, J.G., Mu, J.J., Zhang, L.Q., 2006. Geological character and significance of Adakite and TTG in XiaonangouMingxinggou district in central of Inner Mongolia. Acta Petrological Sinica 22, 2762–2768.

Zhao, G.C., Wilde, S.A., Cawood, P.A., Lu, L., 1999. Tectonothermal history of the basement rocks in the western zone of the North China Craton and its tectonic implications. Tectonophysics 310, 37–53.

Zhao, G.C., Sun, M., Wilde, S.A., Li, S., 2004. A Paleo-Mesoproterozoic supercontinent: assembly, growth and breakup. Earth-Sci. Rev. 67, 91–123.

Zhao, G.C., Sun, M., Wilde, S.A., Sanzhong, L., 2005. Late Archean to Paleoproterozoic evolution of the North China Craton: key issues revisited. Precambr. Res. 136, 177–202.

Zhao, G.C., 2009. Metamorphic evolution of major tectonic units in the basement of the North China Craton: key issues and discussion. Acta Petrological Sinica 25, 1772–1792.

Zhao, G.C., Wilde, S.A., Guo, J., Cawood, P.A., Sun, M., Li, X., 2010. Single zircon grains record two Paleoproterozoic collisional events in the North China Craton. Precambr. Res. 177, 266–276.

Zhao, G.C., Cawood, P.A., 2012. Precambrian geology of China. Precambr. Res. 222, 13–54.

Zheng, J.P., Griffin, W.L., O'Reilly, S.Y.O., Lu, F.X., Wang, C.Y., Zhang, M., Wang, F.Z., Li, H.M., 2004. 3.6 Ga lower crust in central China: new evidence on the assembly of the North China craton. Geology 32 (3), 229–232.

Zheng, J.P., Griffin, W.L., O'Reilly, S.Y.O., Zhao, J.H., Wu, Y.B., Liu, G.L., Pearson, N., Zhang, M., Ma, C.Q., Zhang, Z.H., Yu, C.M., Su, Y.P., Tang, H.Y., 2009. Neoarchean (2.7–2.8 Ga) accretion beneath the North China Craton: U–Pb age, trace elements and Hf isotopes of zircons in diamondiferous kimberlites. Lithos 112, 188–202.

Zhou, H.Y., Mo, X.X., Li, J.J., Li, H.M., 2007. The U–Pb Isotopic Dating Age of Single Zircon from Biotite Plagioclase Gneiss in the Qinggele Area, Alashan, Western Inner Mongolia. Bull. Mineral. Petrol. Geochem. 26, 221–223.

Zhou, X.W., Geng, Y.S., 2009. Metamorphic age of the khondalites in the Helanshan region: constraints on the evolution of the Western block in the North China Craton. Acta Petrological Sinica 25, 1843–1852.

Please cite this article in press as: Wu, S., et al. Petrography and zircon U–Pb isotopic study of the Bayanwulashan Complex: Constrains on the Paleoproterozoic evolution of the Alxa Block, westernmost North China Craton. Journal of Asian Earth Sciences (2014), http://dx.doi.org/10.1016/j.jseaes.2014.05.011